CASL-U-2013-0062-001

Power uprates
and plant life extension

Consortium for Advanced Simulation of LWRs

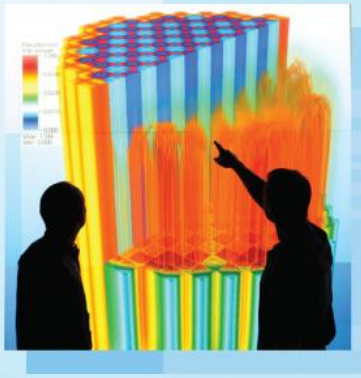

Engineering design
and analysis

L3:THM.CLS.P6.03
ITM/DNS database of drag, lift and wall effects, including the effects of void fractions

J. Fang, A.M. Thomas, I. Bolotnov
J. Lu
G. Tryggvason

North Carolina State University
Worcester Polytechnic Institute
University of Notre Dame

Science-enabling
high performance
computing

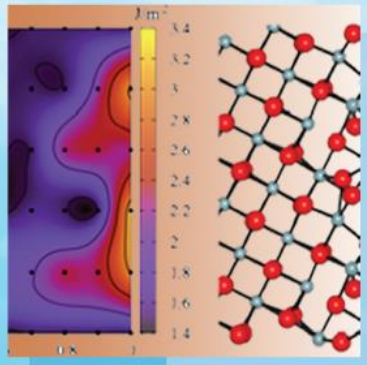

Fundamental science

June 26, 2013

Plant operational data

U.S. DEPARTMENT OF ENERGY | Nuclear Energy

ITM/DNS database of drag, lift and wall effects, including the effects of void fractions

L3:THM.CLS.P6.03 milestone report

Jun Fang[1]
Jiacai Lu[2]
Aaron M. Thomas[1]
Igor A. Bolotnov[1]
Gretar Tryggvason[3]

[1]*North Carolina State University*
[2]*Worcester Polytechnic Institute*
[3]*University of Notre Dame*

June 26, 2013 (Ver. 1.7)

CASL-U-2013-0062-001

Abstract: Interface tracking methods (ITM) are used to examine the lift and drag on a single bubble in vertical shear flow. The effect of the flow parameters, including the shear, the deformability of the bubble, and the distance to the wall are shown and the reversal in lift force as deformability is increased and the distance to the wall is reduced. Results obtained using two different methods are in good agreement with each other as well as with experimental data from the literature. The results demonstrate that lift and drag can be obtained in a reliable way for a wide range of parameters, but strategies for examining a broader range of parameters are identified.

Contents

LIST OF FIGURES 4
LIST OF TABLES 5
1. RELEVANCE TO CASL AND OBJECTIVES 5
2. DESCRIPTION OF NUMERICAL CODES 5
PHASTA *5*
Governing Equations 6
Level Set Method 6
FTC3D *7*
3. ITM CASE DESIGN 8
4. DATA EXTRACTION AND DRAG/LIFT FORCE MEASUREMENT APPROACH 9
5. RESULTS FOR PHASTA SIMULATIONS AND MEASUREMENTS 11
6. RESULTS FOR FTC3D SIMULATIONS AND MEASUREMENTS 29
7. FUTURE WORK 35
BIBLIOGRAPHY 36

List of Figures

Figure 1. The front tracking code uses a fixed structured grid for the solution of the fluids equation and an unstructured surface grid to track the interface between the different fluids. 7
Figure 2. Summary of the S1/R25 case with uniform shear of 1.0. Top left shows sample of velocity distribution around the bubble, bottom left and right: control force evolution in horizontal and vertical directions, respectively. Top right shows basic case parameters and lift/drag coefficient evaluation results..... 13
Figure 3. Summary of the S2 case with uniform shear of 2.0. 14
Figure 4. Summary of the S5 case with uniform shear of 5.0. 15
Figure 5. Summary of the S10 case with uniform shear of 10.0. 16
Figure 6. Summary of the S50 case with uniform shear of 50.0. 17
Figure 7. Summary of the R50 case with uniform shear of 1.0 with increase relative velocity. 18
Figure 8. Summary of the R100 case with uniform shear of 1.0 with even higher relative velocity. 19
Figure 9. Summary of the NSW1 case with uniform shear of 2.0. Bubble is located 1 radius from the top no-slip wall. 20
Figure 10. Summary of the SW1 case with uniform shear of 2.0. Bubble is located 1 radius from the top free-slip wall. 21
Figure 11. Summary of the NSW0.5 case with uniform shear of 2.0. Bubble is located half the radius from the top no-slip wall. 22
Figure 12. Summary of the SW0.5 case with uniform shear of 2.0. Bubble is located half the radius from the top free-slip wall. 23
Figure 13. Summary of the NSW0.25 case with uniform shear of 2.0. Bubble is located one quarter of the radius from the top no-slip wall. 24
Figure 14. Summary of the ONSW1 case with uniform shear of 2.0. Bubble is located one radius from the bottom no-slip wall. Top part of the domain was cut off to show the details and legend. 25
Figure 15. Summary of the ONSW0.5 case with uniform shear of 2.0. Bubble is located half the radius from the bottom no-slip wall. 26
Figure 16. Summary of the ONSW0.25 case with uniform shear of 2.0. Bubble is located a quarter of the radius from the bottom no-slip wall. 27
Figure 17. Lift coefficient dependence on the distance from the wall (measured in bubble radii from the closest point of the interface to the wall). Red line shows the slip-wall condition option. 28
Figure 18. The bubble and the velocity field shown by a quiver plot. The color indicates the vertical velocity component. In the left frame the bubble is in the middle of the domain and in the right frame the bubble is close to the right wall. 32
Figure 19. The horizontal (top) and the vertical (bottom) component of the gravitational acceleration versus time, as adjusted by the PID controllers to keep the bubble stationary. 33
Figure 20. The lift and drag coefficients versus the Eotvos (Eo) number. 34
Figure 21. The lift (a) and drag (b) coefficient versus shear rate. 34
Figure 22. The effect of the distance to the wall on the lift (a) and drag (b) force on the bubbles. 34
Figure 23. The effect of the distance to the wall on the lift (a) and drag (b) force on the bubbles for a bubble Reynolds number = 50. 35

List of Tables

Table 1. PHASTA mesh / simulation parameters 12
Table 2. The various parameters used for the FTC3D baseline case. 31

1. Relevance to CASL and Objectives

Development and validation of closure laws for computational multiphase fluid dynamics (CMFD) is a necessary part of successful prediction of reactor thermal hydraulics behavior. The presented study demonstrates the capabilities of the advanced numerical tools to determine the essential closure parameters in a range of conditions. Further studies can enhance the parametric space and fill in the gaps in the available experimental database.

2. Description of numerical codes

PHASTA

PHASTA is a parallel, hierarchic, higher-order accurate (from the 2nd to the 5th order accuracy, depending on function choice), adaptive, stabilized (finite element) transient analysis flow solver (both incompressible and compressible). This approach has been shown by (Jansen, 1999) and (Whiting & Jansen, 2001) to be an effective tool for bridging a broad range of length scales in turbulent (RANS, large-eddy simulation (LES), detached eddy simulation (DES), DNS) flows. PHASTA (and its predecessor, ENSA) was the first unstructured grid LES code (Jansen, 1993) and has been applied to turbulent flows ranging from validation benchmarks (channel flow, decay of isotropic turbulence) to complex flows (airfoils at maximum lift, flow over a cavity, near lip jet engine flows and fin-tube heat exchangers). The PHASTA code uses advanced anisotropic adaptive algorithms (Sahni, et al., 2006) and the most advanced LES/DES models (Tejada-Martinez & Jansen, 2005). Note that DES, LES, and DNS are computationally intensive even for single phase flows. This capability has been recently (Nagrath, et al., 2006) extended to two phase flows where we use the level set method to track the boundary between two immiscible fluids (either compressible - where we captured new instabilities in sonoluminescence, or incompressible – to study bubble coalescence and two-phase turbulence (Bolotnov, et al., 2011)). PHASTA uses anisotropically adapted unstructured grids and its highly scalable performance on massively parallel computers has already been demonstrated (the code has shown good scaling out to 288*1024 IBM Blue Gene processors, at JUGENE, BG/P (Germany, #12 in top500 as of June 2011)), (Zhou, et al., 2010).

PHASTA is an *open source* code. However, in the current setup, it uses commercial linear solver libraries from Acusim, Inc. A possible switch to open-source solvers is considered (e.g. Trilinos, PETSc). Meshing

capabilities utilize tools from Simmetrix, Inc. Creating mesh converters from open-source tools to PHASTA format is also a possibility. PHASTA works with hexahedral, tetrahedral and mixed meshes.

Governing Equations

The spatial and temporal discretization of the Incompressible Navier-Stokes (INS) equations within the FEM code PHASTA has been described in (Whiting & Jansen, 2001) and (Nagrath, et al., 2006). The strong form of the INS equations is given by:

Continuity: $$u_{i,i} = 0 \quad (1)$$

Momentum: $$\rho u_{i,t} + \rho u_j u_{i,j} = -p_{,i} + \tau_{ij,j} + f_i \quad (2)$$

For the incompressible flow of a Newtonian fluid, the viscous stress tensor is related to the fluid's viscosity and the strain rate tensor as:

$$\tau_{ij} = 2\mu S_{ij} = \mu(u_{i,j} + u_{j,i}) \quad (3)$$

Using the Continuum Surface Tension (CST) model of (Brackbill, et al., 1992), the surface tension force is computed as a local interfacial force density, which is included in f_i.

Level Set Method

The level set method of Sussman [(Sussman & Fatemi, 1999), (Sussman & Smereka, 1997), (Sussman, et al., 1999), (Sussman, et al., 1998)] and (Sethian, 1999) involves modeling the interface as the zero-level set of a smooth function, φ, where φ is often called the first scalar and it represents the signed distance from the interface. Hence, the interface is defined by $\varphi = 0$. The scalar, φ, is convected within a moving fluid according to,

$$\frac{D\varphi}{dt} = \frac{\partial \varphi}{\partial t} + \underline{u} \cdot \nabla \varphi = 0 \quad (4)$$

where $\underline{u}$ is the flow velocity vector. Phase-1, the liquid phase, is indicated by a positive level set, $\varphi > 0$, and phase-2, the gas, by a negative level set, $\varphi < 0$. Since evaluating the jump in physical properties using a step change across the interface leads to poor computational results, the properties near an interface were defined using a smoothed Heaviside kernel function, H_ε, given by (Sussman, et al., 1999):

$$H_\varepsilon(\varphi) = \begin{cases} 0 & ,\varphi < -\varepsilon \\ \frac{1}{2}\left[1 + \frac{\varphi}{\varepsilon} + \frac{1}{\pi}\sin\left(\frac{\pi\varphi}{\varepsilon}\right)\right] & ,|\varphi| < \varepsilon \\ 1 & ,\varphi > \varepsilon \end{cases} \quad (5)$$

The fluid properties are then defined as:

$$\rho(\varphi) = \rho_1 H_\varepsilon(\varphi) + \rho_2(1 - H_\varepsilon(\varphi)) \quad (6)$$

$$\mu(\varphi) = \mu_1 H_\varepsilon(\varphi) + \mu_2(1 - H_\varepsilon(\varphi)) \quad (7)$$

Although the solution may be reasonably good in the immediate vicinity of the interface, the distance field may not be correct throughout the domain since the varying fluid velocities throughout the flow field distort the level set contours (especially in fully resolved turbulent flow simulations). Thus, the level set was corrected with a re-distancing operation by solving the following PDE (Sussman & Fatemi, 1999):

$$\frac{\partial d}{\partial \tau} = S(\varphi)\left[1 - |\nabla d|\right] \qquad (8)$$

where *d* is a scalar that represents the corrected distance field and τ is the pseudo time over which the PDE is solved to steady-state. This may be alternately expressed as the following transport equation:

$$\frac{\partial d}{\partial \tau} + \underline{w} \cdot \nabla d = S(\varphi) \qquad (9)$$

The so-called second scalar, *d*, is originally assigned the level set field, *φ*, and is convected with a pseudo velocity, $\underline{w}$, where,

$$\underline{w} = S(\varphi)\frac{\nabla d}{|\nabla d|} \qquad (10)$$

and *S(φ)* is defined as:

$$S(\varphi) = \begin{cases} -1 & , \varphi < -\varepsilon_d \\ \left[\dfrac{\varphi}{\varepsilon_d} + \dfrac{1}{\pi}\sin\left(\dfrac{\pi\varphi}{\varepsilon_d}\right)\right] & , |\varphi| < \varepsilon_d \\ 1 & , \varphi > \varepsilon_d \end{cases} \qquad (11)$$

where ε_d is the distance field interface half-thickness which, in general, may be different from ε used in Eq. (5). Note that the zeroth level set, or interface, *φ = 0*, does not move since its convecting velocity, $\underline{w}$, is zero. Solving the second scalar to steady-state restores the distance field to $\nabla d = \pm 1$ but does not alter the location of the interface. The first scalar, *φ*, is then updated using the steady solution of the second scalar, *d*.

FTC3D

FTC3D is a specialized code for direct numerical simulations of multiphase flows. The "one-fluid" Navier-Stokes equations for incompressible flows, where a single set of equations is used for the whole flow domain, are solved on a regular structured staggered grid using an explicit projection method. Time integration is done by a second order predictor-corrector method, the viscous terms are discretized by second-order centered differences and the advection terms are approximated using a QUICK scheme. The pressure equation is solved using a multigrid method or a Krylov scheme (BIGSTAB).

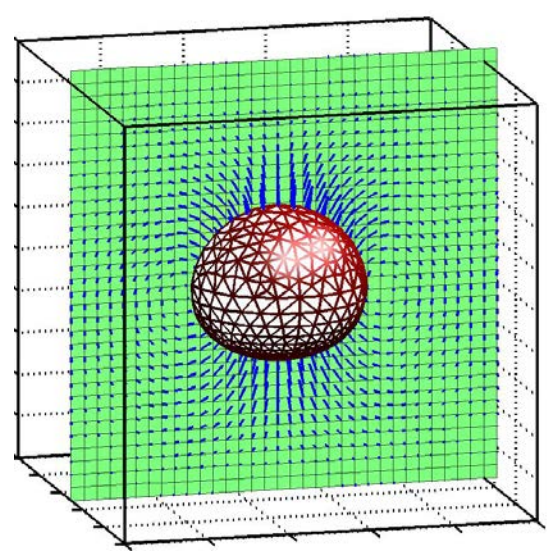

Figure 1. The front tracking code uses a fixed structured grid for the solution of the fluids equation and an unstructured surface grid to track the interface between the different fluids.

The interface between the different fluids is tracked by connected marker points that are advected with the flow. The interface, or the "front," consists of points and triangular elements that connect the points. Once the marker points have been advected, a marker function is constructed from the new

interface location. The front is also used to compute surface tension, which is then smoothed onto the fluid grid and added to the discrete Navier-Stokes equations. In addition to the computation of the surface tension and the construction of the marker function, the chief challenge in front-tracking is the dynamic updating of the front, whereby marker points are added or deleted to maintain the point density needed to fully resolve the interface. This is done fully automatically as part of the front advection.

The method was introduced by Unverdi & Tryggvason (1992) and for description of the original method, as well as various improvements and refinements, see Tryggvason et al. (2001) and Tryggvason et al. (2011). The method has been used to simulate a large range of multiphase flows, including bubbly flows. See, Bunner & Tryggvason (2002a,b), Esmaeeli & Tryggvason (2005), and Biswas, Esmaeeli & Tryggvason (2005), for example. For other implementation of similar ideas and applications to bubbly flows, see Dijkhuizen et al. (2010a,b); van Sint Annaland et al. (2006); Hao & Prosperetti (2004); Hua & Lou (2007); Muradoglu & Kayaalp (2006), for example.

3. ITM Case design

In order to provide the lift coefficient estimate in clean uniform shear flow it was decided to use inflow/ouflow boundary conditions. This provides a better liquid flow field around the bubble compared to more conventional periodic boundary conditions in stream-wise direction. Uniform shear inflow avoids having the bubble traveling through its own wake and disturbing the measurements of lift/drag forces.

Figure 2 shows the slice of the computational domain (normal to z-axis) and provides a basic idea how the simulations were performed. To achieve the uniform shear flow around the bubble uniform velocity boundary condition was applied on each wall (in this particular case with values of 0.0375 on the top and 0.0125 on the bottom) along with uniform shear inflow boundary condition on the left. The domain width of 0.025 results in the shear rate of 1.0 s^{-1} for this case.

The following procedure has been used to obtain the results:

- the bubble is introduced in the level set method by specifying an analytical expression for a distance field:

$$\varphi_i = \left(x - x_j\right)^2 + \left(y - y_j\right)^2 + \left(z - z_j\right)^2 - R_j^2 \qquad (12)$$

  where x_j, y_j, z_j are the coordinates of the bubble and R_j is the radius.
- two control forces (applied independently) in x and y directions were used to keep the bubble location nearly constant. After achieving steady-state results the x-direction force fully counter-acts the drag force the bubble experiencing due to upcoming flow and the y-direction force counter-acts the lift force.
- the simulation is carried out to acquire sufficient data for convergent results in control force evolution.

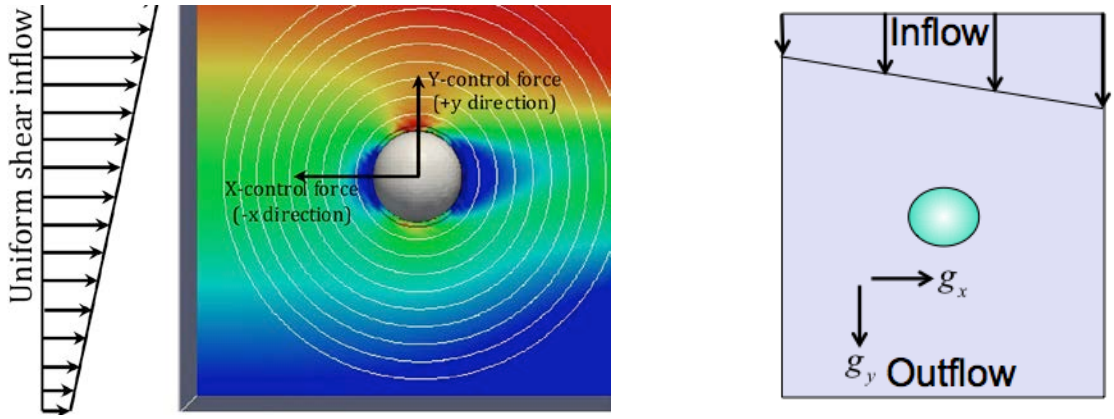

Figure 2. Simulation domain and control forces. Left: Setup and coordinates for the PHASTA runs. Right: Setup and coordinates for the FTC3D runs.

4. Data extraction and drag/lift force measurement approach

The computational domain used in the FTC3D runs is a rectangular channel where the inflow at the top is specified, the left and right boundaries are rigid no-slip walls with a given velocity and periodic boundary conditions are used in the spanwise direction. The computational domain, shown in Figure 2, is the same as used for the PHASTA simulations but the orientation and notation is slightly different.

To keep the bubble stationary, the gravity is adjusted by a PID (proportional-integral-derivative) controller based on the location and velocity of the bubble centroid. At every time step, the new values are found by:

$$\begin{aligned} g_x^{\alpha+1} &= g_x^{\alpha} - c_{Px}\left(x - x_0\right) - c_{Ix}\int\left(x - x_0\right)dt - c_{Dx}U_b \\ g_y^{\alpha+1} &= g_y^{\alpha} - c_{Py}\left(y - y_0\right) - c_{Iy}\int\left(y - y_0\right)dt - c_{Dx}V_b \end{aligned} \qquad (13)$$

For most of the calculations reported in the section on FTC3D, we use the following control parameters:

$$\begin{aligned} c_{Px} &= 0.02;\ c_{Ix} = 0.01;\ c_{Dx} = 0.02 \\ c_{Py} &= 0.03;\ c_{Iy} = 0.02;\ c_{Dy} = 0.05 \end{aligned} \qquad (14)$$

Once gravity acceleration has been determined, the lift and drag coefficients can be determined by balancing the buoyancy and lift or drag. PHASTA used the same approach, with slightly different coefficients for some cases.

For the FTC3D results we do so in the following way. The lift force is given by:

$$F_L = -C_L\rho\frac{\pi d^3}{6}\left(V_b - V_L\right)\times\Omega_L \text{ where } \left|\Omega_L\right| = \frac{\Delta V}{L} \qquad (15)$$

The buoyancy force in the horizontal direction is:

$$F_B = \Delta\rho\frac{\pi d^3}{6}g_x$$

$$F_L = -C_L \rho \frac{\pi d^3}{6}\left(V_b - V_L\right) \times \Omega_L \text{ where } \left|\Omega_L\right| = \frac{\Delta V}{L} \quad (16)$$

and at steady state the buoyancy balances the lift, $F_B = F_L$. We can isolate the lift coefficient, resulting in:

$$C_L = \frac{\Delta\rho g_x L}{\rho V_L \Delta V} \text{ where } \left|\Omega_L\right| = \frac{\Delta V}{L} \quad (17)$$

Similarly, the drag in the vertical direction is:

$$F_D = C_D \frac{\pi d^2}{8} \rho V_b^2 \quad (18)$$

which must be balanced by buoyancy in the vertical direction. Thus

$$C_D = \frac{4}{3}\frac{d\Delta\rho g_y}{\rho V_b^2} \quad (19)$$

The various non-dimensional numbers are defined as:

$$\mathrm{Re} = \frac{\rho d V_b}{\mu}; \quad Eo = \frac{\Delta\rho g d^2}{\sigma}; \quad M = \frac{\Delta\rho g \mu^4}{\rho^2 \sigma^3}; \quad G = \frac{\rho d^2}{\mu}\frac{\Delta V}{L}; \quad (20)$$

PHASTA

The value which is extracted by overall control forces in PHASTA code is measured in [N/kg], and it's the corresponding buoyancy forces due to the 'control forces' that balance lift force and drag force. We use the following lift force formula (Tomiyama, et al., 2002):

$$F_{LF} = -C_{LF} \rho_L V_b \left(V_G - V_L\right) \times rotV_L \quad (21)$$

where

$$\left|rotV_L\right| = \left|\frac{dV_L}{dy}\right|, \ \left|v_r\right| = \left|V_G - V_L\right| \quad (22)$$

in our cases. The drag equation is given by

$$F_D = \frac{1}{2} C_D \rho_L v_r^2 A \quad (23)$$

The half thickness of the interface (applicable for level set method approach only) is determined in the following way

$$r = \frac{d}{\gamma_d} \cdot \varepsilon \quad (24)$$

where the *d* is the bubble diameter, γ_d is the resolution across bubble diameter and ε is the number of elements across the half interface.

The density distribution of the interface can be described by Eqs. (5) and (6). The average density within the blended level-set interface is:

$$\overline{\rho}_s = \frac{\rho_L + \rho_G}{2} \quad (25)$$

The volume of gas only region is

$$V_G = \frac{4}{3}\pi\left(R_b - r\right)^3 \qquad (26)$$

and the volume of the interface region is

$$V_s = \frac{4}{3}\pi\left(R_b + r\right)^3 - \frac{4}{3}\pi\left(R_b - r\right)^3 \qquad (27)$$

In the x direction (stream-wise), the force balance is given by

$$F_D = \left|g + xcf\right|\left[\left(\rho_L - \rho_G\right)V_G + \left(\rho_L - \bar{\rho}_s\right)V_s\right] = \frac{1}{2}C_D\rho_L v_r^2 A \qquad (28)$$

And in y direction, the force balance is

$$F_{LF} = \left|ycf\right|\left[\left(\rho_L - \rho_G\right)V_G + \left(\rho_L - \bar{\rho}_s\right)V_s\right] = C_{LF}\rho_L V_b \left|v_r\right|\left|\frac{dv}{dy}\right| \qquad (29)$$

After getting the *xcf* and *ycf*, we have calculated the corresponding coefficients based on the above equations. For instance, in the case for shear rate is 1.0 the average 'y control force' for timesteps 1000 to 3000 is *ycf*=0.0116; the lift coefficient calculated is 0.3441. The average 'x control force' from timestep 1000 to timestep 6000 is xcf=-0.0311; the drag coefficient calculated is 0.6105.

5. Results for PHASTA simulations and measurements

Table 1 summarizes the presented simulations done using the PHASTA-ITM code. We will overview selected cases to present more detailed results about the bubble behavior. 3 basic studies were performed to evaluate the influence of the shear rate; influence of relative velocity and influence of the wall presence on the estimates of the lift and drag coefficients.

Shear rate influence was evaluated using the "S" group of simulations: S1, S2, S5 and S10 representing the bubble in shear rates of 1, 2, 5 and 10. We have observed a decreased lift coefficient for higher shear rates. Note that S5 and S10 cases used partially negative inflow boundary conditions to obtain a combination of low relative velocity and high shear rates in a domain with fixed bubble position.

Relative velocity influence on both lift and drag was studied by increasing the velocity of both walls while maintaining the same shear rate. The set of cases designated by "R" was performed: R25; R50; R100.

Third study involved evaluating the influence of the wall on the lift force. For the specific set of conditions the wall proximity resulted in an increase of the lift coefficient since original direction of the lift force was away from the top wall (similar to downflow conditions). We have investigated both no-slip and free-slip walls (NSW and SW cases) to quantify the effect of the wall friction on the liquid "blockage" of the bubble and assist the development of the new closure laws for lift forces near solid boundaries.

Table 1. PHASTA mesh / simulation parameters

Case studies		Description	Results
Shear rate study	S1: $\frac{dv}{dy} = 1.0$	Uniform shear of 1.0; relative velocity of 0.025; bubble is located in the center of the domain. Domain width is 5 bubble diameters. Bubble diameter is 5mm	$C_{lift} = 0.3441$; $C_{drag} = 0.6105$
	S2: $\frac{dv}{dy} = 2.0$	Uniform shear of 2.0; relative velocity of 0.05	$C_{lift} = 0.3523$; $C_{drag} = 0.2089$
	S5: $\frac{dv}{dy} = 5.0$	Uniform shear of 5.0; relative velocity of 0.05	$C_{lift} = 0.2342$; $C_{drag} = 0.2057$
	S10: $\frac{dv}{dy} = 10.0$	Uniform shear of 10.0; relative velocity of 0.05	$C_{lift} = 0.2118$; $C_{drag} = 0.2322$
	S50: $\frac{dv}{dy} = 50.0$	Uniform shear of 50.0; relative velocity of 0.05. Bubble of 0.1 mm.	*in progress*
Relative velocity studies ($\frac{dv}{dy} = 1.0$)	R25: $V_r = 0.025$	Identical to S1	$C_{lift} = 0.3441$; $C_{drag} = 0.6105$
	R50: $V_r = 0.050$	Uniform shear of 1.0; relative velocity of 0.05	$C_{lift} = 0.3248$; $C_{drag} = 0.1932$
	R100: $V_r = 0.100$	Uniform shear of 1.0; relative velocity of 0.1	$C_{lift} = 0.5021$; $C_{drag} = 0.1013$
No-slip wall effect study	NSW1:	"No Slip Wall" study. Uniform shear of 2.0; Bubble is located at 1 radius distance (measured from the top bubble surface towards the top wall); relative velocity of 0.065	$C_{lift} = 0.3016$; $C_{drag} = 0.1411$
	SW1:	"Slip Wall" case. Uniform shear of 2.0; relative velocity of 0.065. The top wall is free slip boundary condition to allow free flow of liquid in the blockage region between the bubble and the wall.	$C_{lift} = 0.2952$; $C_{drag} = 0.1396$
	NSW0.5:	Reduced distance between the bubble and the wall compared to NSW1 (half the radius). Relative velocity in this case: 0.0675	$C_{lift} = 0.4888$; $C_{drag} = 0.1440$
	SW0.5:	Reduced distance between the bubble and the wall compared to SW1 (half the radius). Relative velocity in this case: 0.0675	$C_{lift} = 0.4544$; $C_{drag} = 0.1374$
	NSW0.25:	Reduced distance between the bubble and the wall compared to NSW1 (quarter the radius). Relative velocity in this case: 0.06875	$C_{lift} = 0.7733$; $C_{drag} = 0.1754$
	ONSW1:	Uniform shear of 2.0; Bubble is located at 1 radius distance (measured from the bottom bubble surface towards the opposite/bottom wall); relative velocity of 0.065 (wall velocities: 0.055, 0.105)	$C_{lift} = 0.1938$; $C_{drag} = 0.1756$
	ONSW0.5:	Reduced distance between the bubble and the wall compared to ONSW1 (half the radius). Relative velocity in this case: 0.0675 (wall velocities: 0.06, 0.11)	$C_{lift} = 0.0192$; $C_{drag} = 0.1258$
	ONSW0.25:	Reduced distance between the bubble and the wall compared to ONSW1 (quarter the radius). Relative velocity in this case: 0.06875 (wall velocities: 0.0625, 0.1125)	$C_{lift} = -0.1697$; $C_{drag} = 0.0803$

Case S1/R25: The detailed information for each case will be summarized in a table.

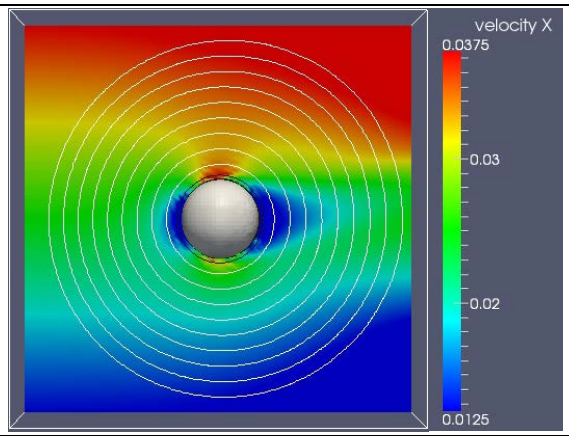

Shear rate: 1.0 s^{-1}
Relative velocity: 0.025 m/s
Density: 996.5/1.161 (kg/m^3)
Viscosity: 8.5439E-04 (liquid); 1.858E-05 (gas)
Bubble diameter: 5 mm
Eo/Bo number: 0.0782
Force estimate is over timestep range of: 1000 - 3000
Drag control force: 0.0689 N/kg
Lift control force: 0.0116 N/kg
Drag coefficient: 0.6105
Lift coefficient: 0.3441

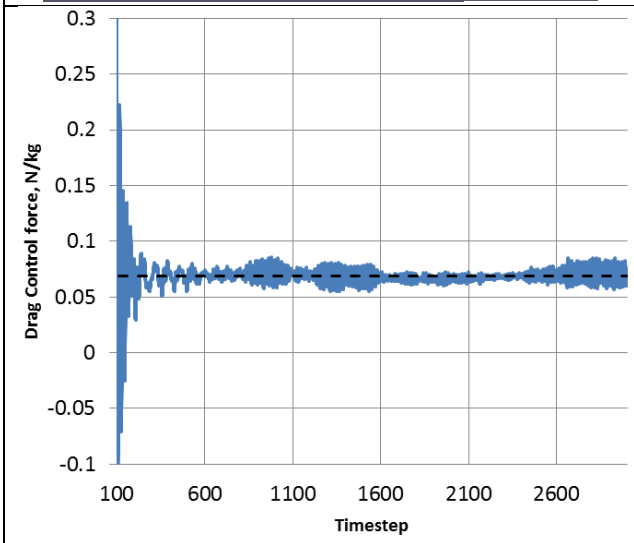

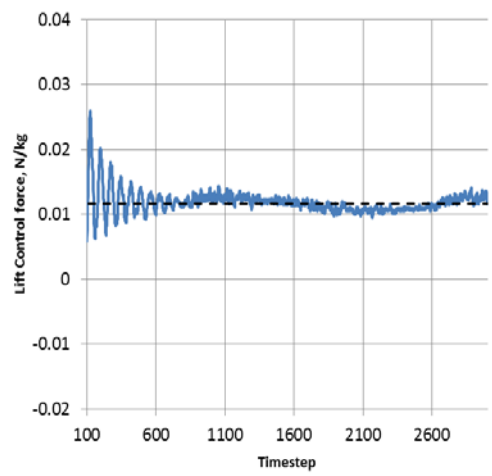

Figure 2. Summary of the S1/R25 case with uniform shear of 1.0. Top left shows sample of velocity distribution around the bubble, bottom left and right: control force evolution in horizontal and vertical directions, respectively. Top right shows basic case parameters and lift/drag coefficient evaluation results.

Case S2:

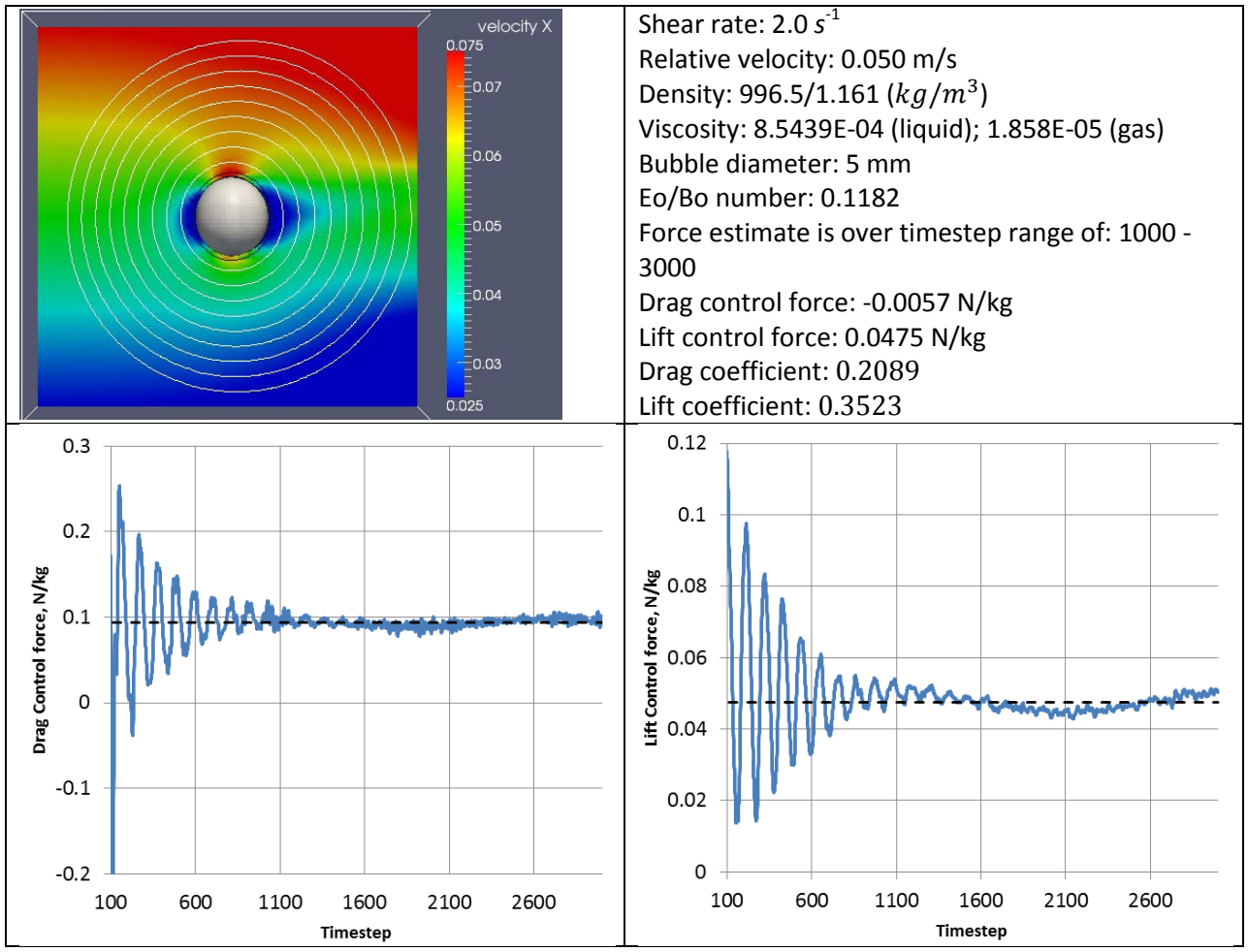

Figure 3. Summary of the S2 case with uniform shear of 2.0.

Case S5:

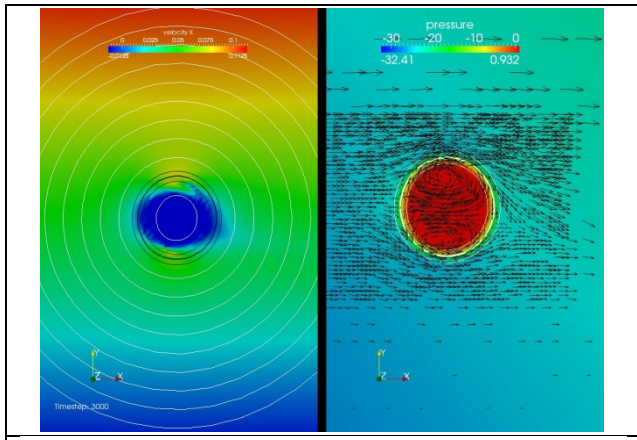

Shear rate: 5.0 s^{-1}
Relative velocity: 0.050 m/s
Density: 996.5/1.161 (kg/m^3)
Viscosity: 8.5439E-04 (liquid); 1.858E-05 (gas)
Bubble diameter: 5 mm
Eo/Bo number: 0.1077
Force estimate is over timestep range of: 1000 - 3000
Drag control force: 0.0919 N/kg
Lift control force: 0.0775 N/kg
Drag coefficient: 0.2057
Lift coefficient: 0.2342

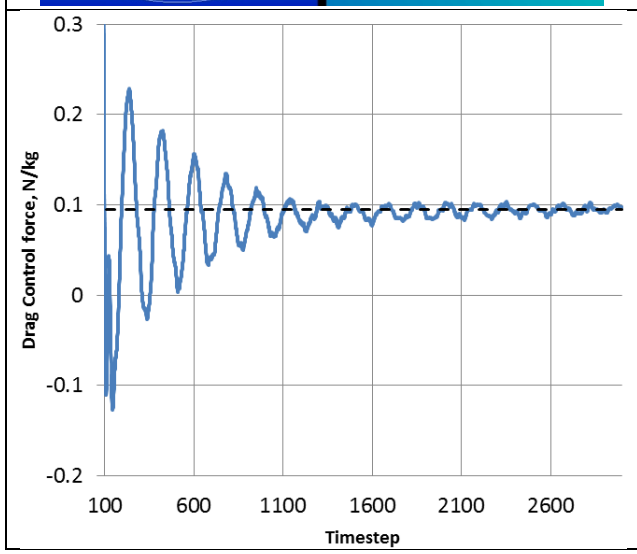

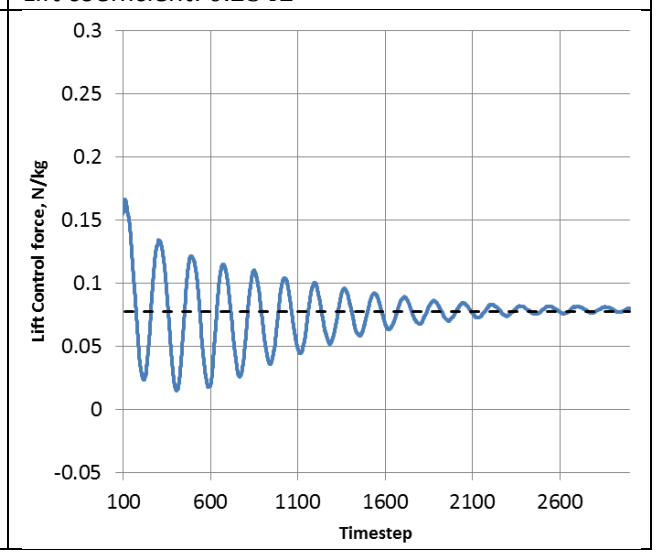

Figure 4. Summary of the S5 case with uniform shear of 5.0.

Case S10:

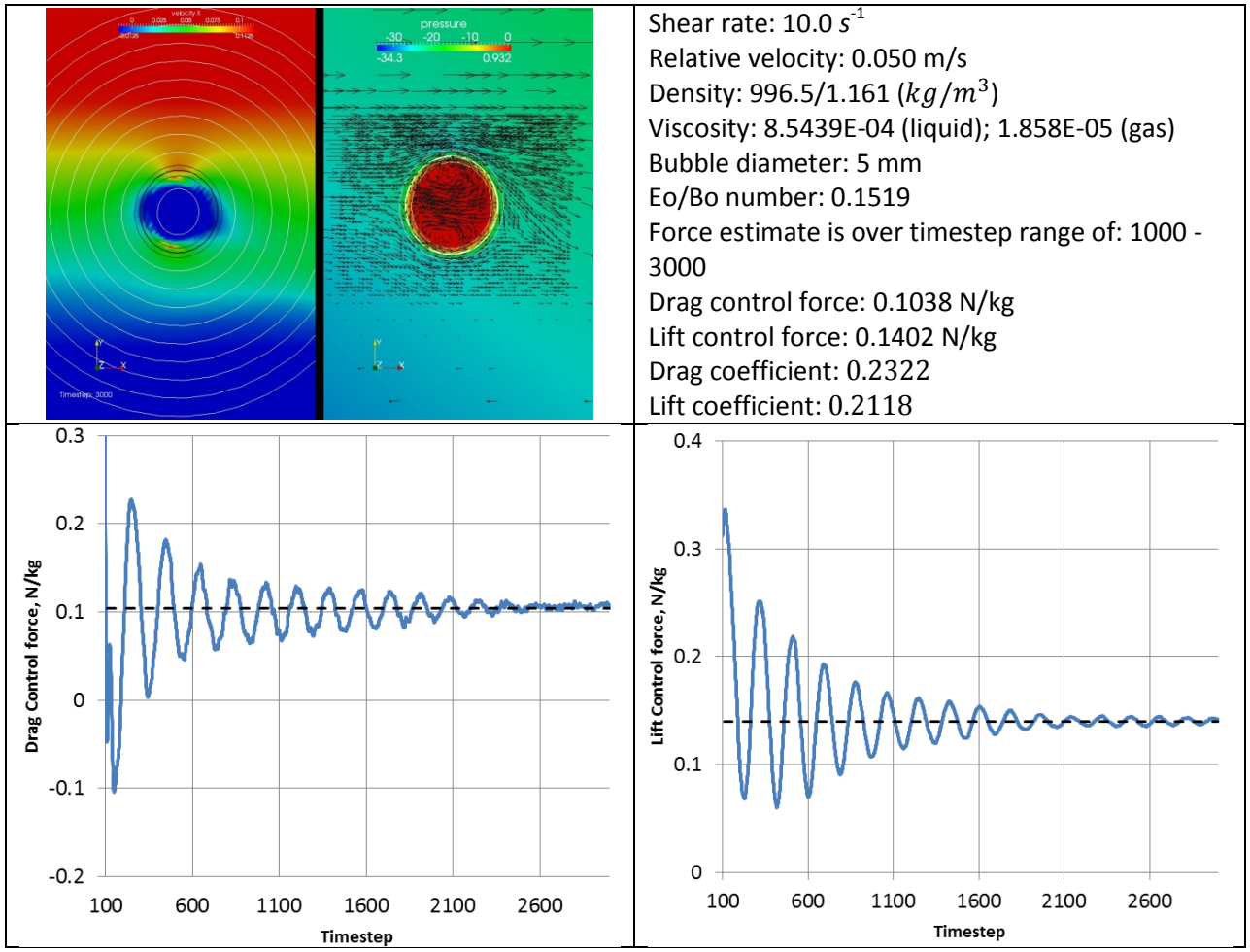

Figure 5. Summary of the S10 case with uniform shear of 10.0.

Figure 6 demonstrated the ITM capabilities of resolving the high shear rate flows (still laminar at this time) with low relative velocity. In LWR conditions we expect similar behavior since the relative velocity of the bubble is controlled by the balance of drag and buoyancy forces and will be fairly small (case S50 is performed for 0.1mm bubble). However, the shear rate is expected to reach values of 1000 or more. The tested capability as part of this effort demonstrated that applying fixed velocity boundary conditions for both “inflow” and “outflow” with negative portions in each outlet is possible without any adverse effects on code convergence. Note the velocity field shown with vectors in Figure 6.

<u>Case S50</u>: Shear rate study.

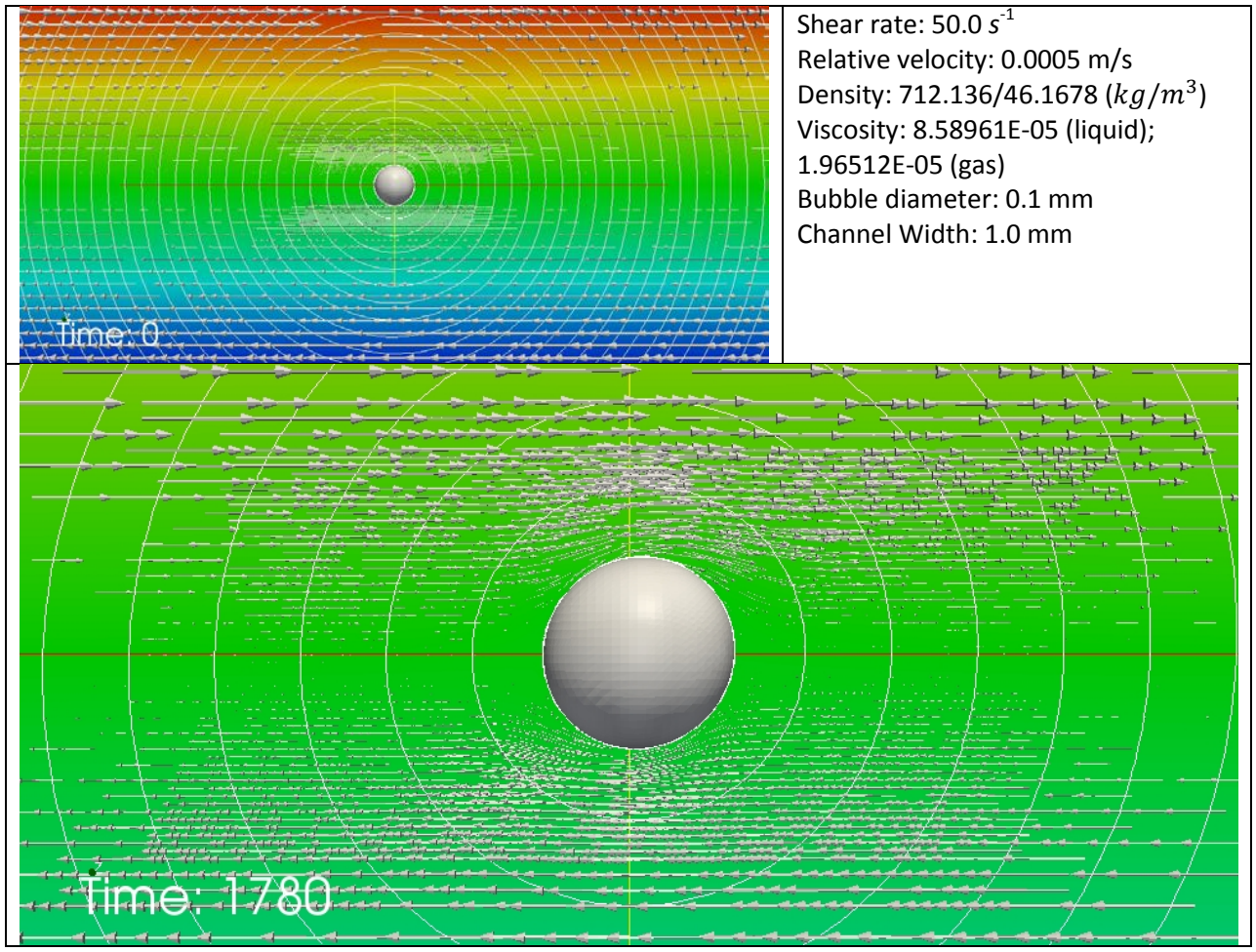

Figure 6. Summary of the S50 case with uniform shear of 50.0.

Case R50: Relative velocity study.

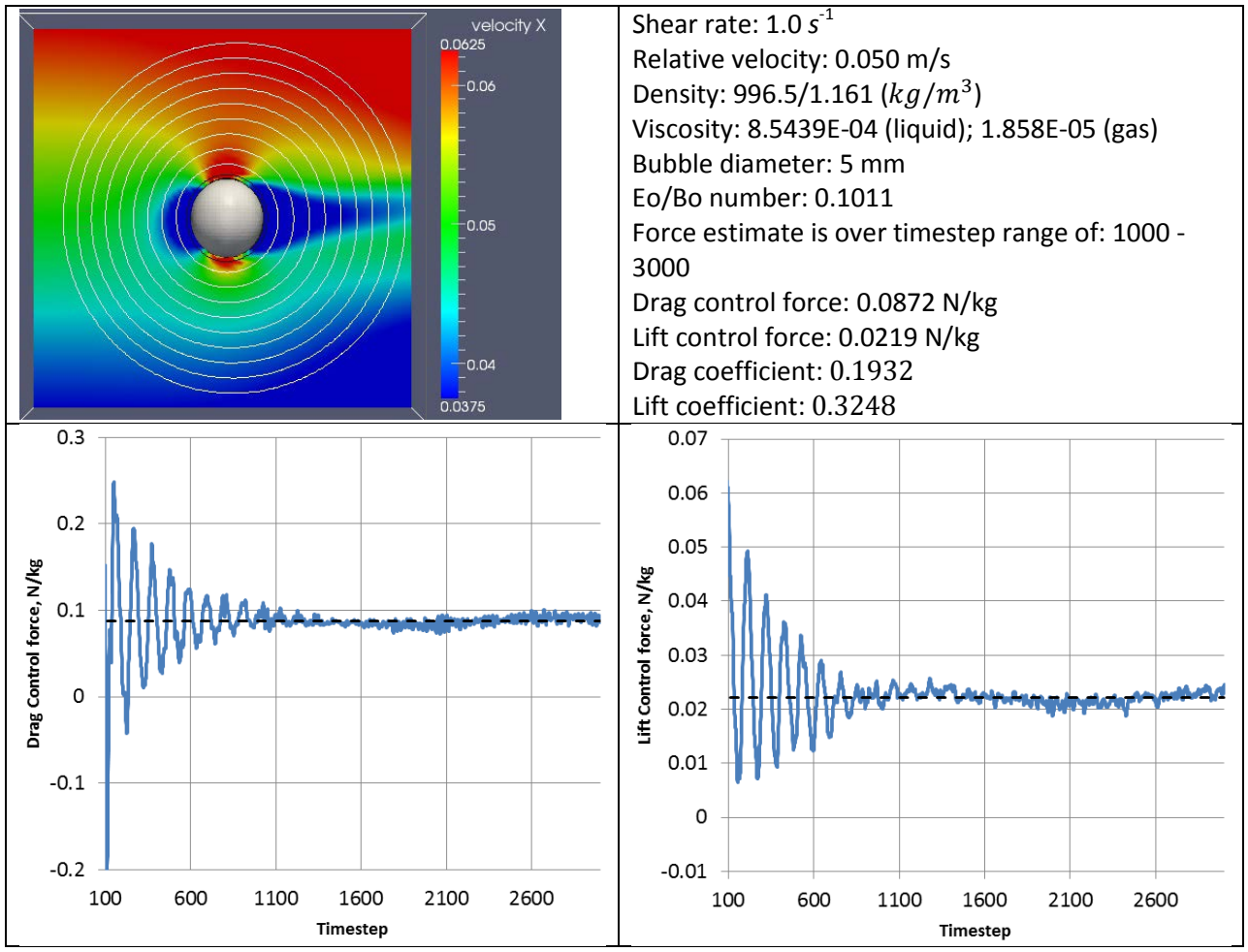

Figure 7. Summary of the R50 case with uniform shear of 1.0 with increase relative velocity.

Case R100: Relative velocity study.

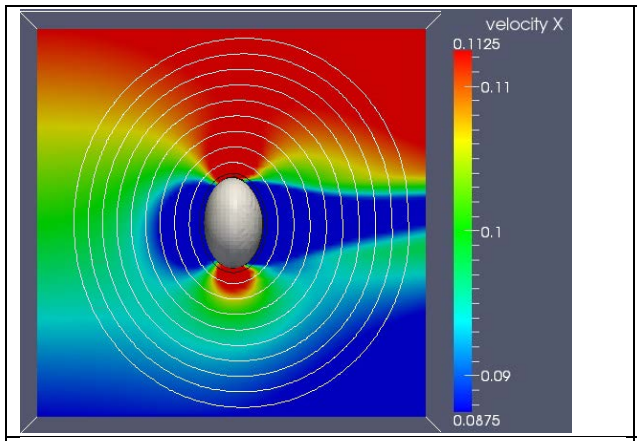

Shear rate: 1.0 s^{-1}
Relative velocity: 0.100 m/s
Density: 996.5/1.161 (kg/m^3)
Viscosity: 8.5439E-04 (liquid); 1.858E-05 (gas)
Bubble diameter: 5 mm
Eo/Bo number: 0.2185
Force estimate is over timestep range of: 1000 - 3000
Drag control force: 0.1830 N/kg
Lift control force: 0.0677 N/kg
Drag coefficient: 0.1013
Lift coefficient: 0.5021

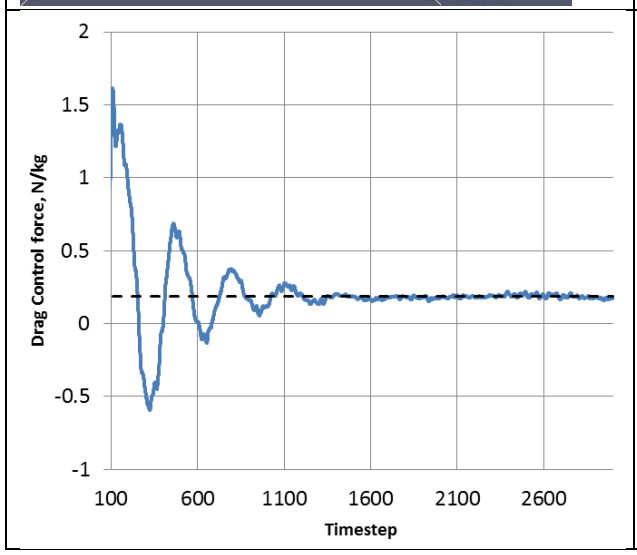

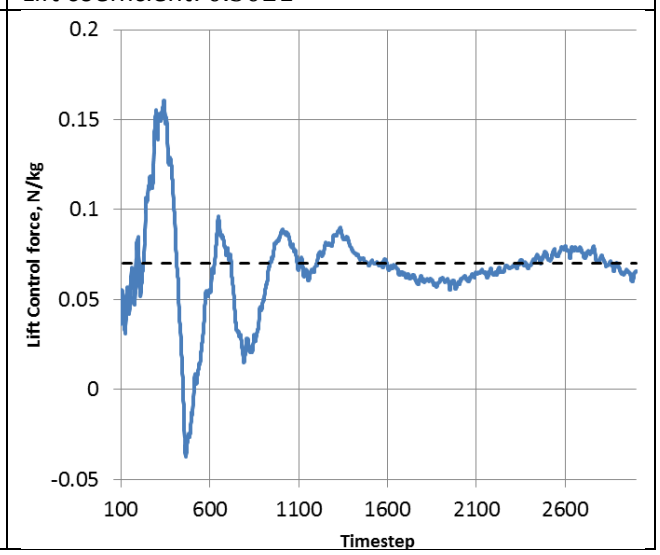

Figure 8. Summary of the R100 case with uniform shear of 1.0 with even higher relative velocity.

<u>Case NSW1</u>: The detailed information for this case is summarized in the following table.

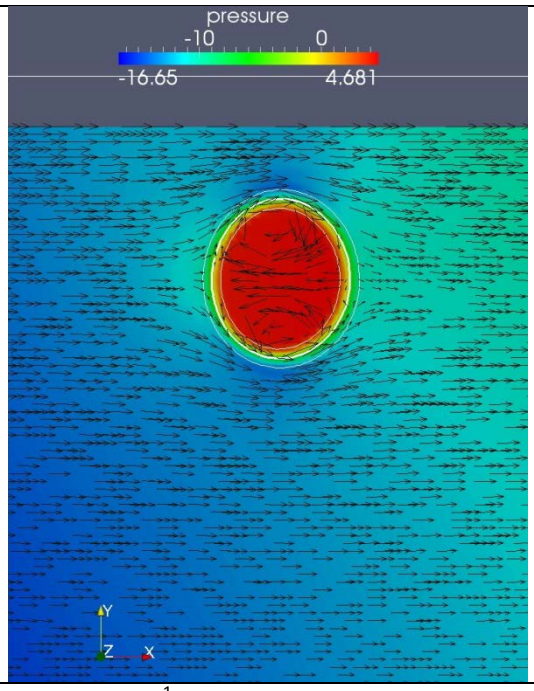

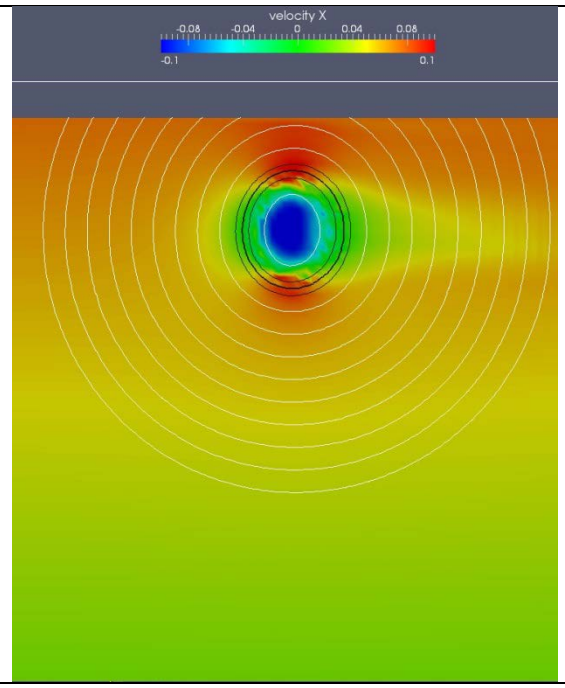

Shear rate: 2.0 s^{-1}
Relative velocity: 0.065 m/s
Density: 996.5/1.161 (kg/m^3)
Viscosity: 8.5439E-04 (liquid); 1.858E-05 (gas)
Bubble diameter: 5 mm

Force averaging range: 1000 - 3000
Drag control force: 0.10768 N/kg
Lift control force: 0.05286 N/kg
Drag coefficient: 0.1411
Lift coefficient: 0.3016

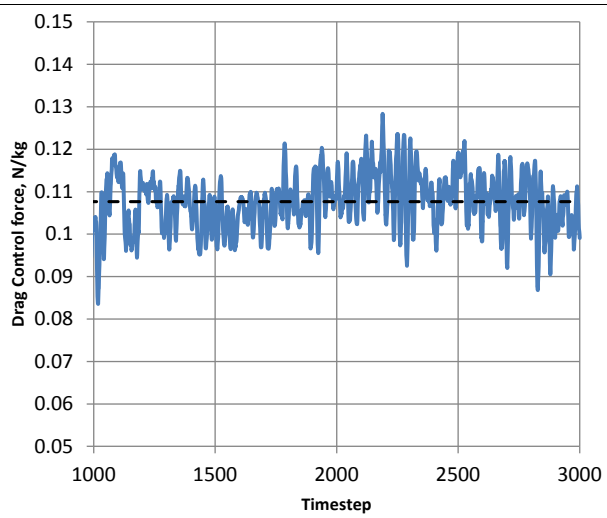

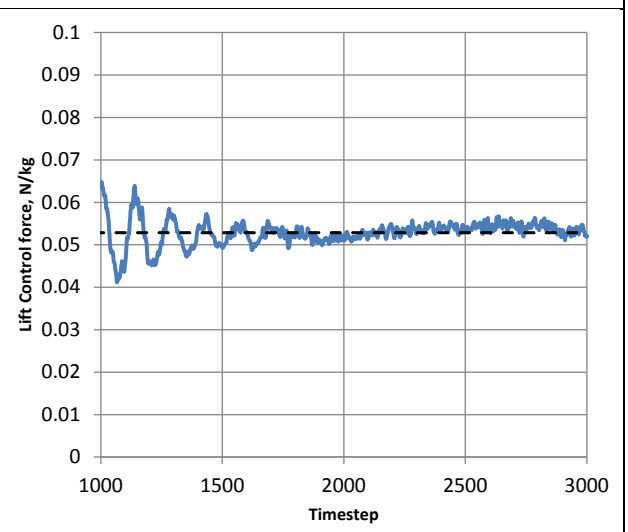

Figure 9. Summary of the NSW1 case with uniform shear of 2.0. Bubble is located 1 radius from the top no-slip wall.

<u>Case SW1</u>: The detailed information for this case is summarized in the following table.

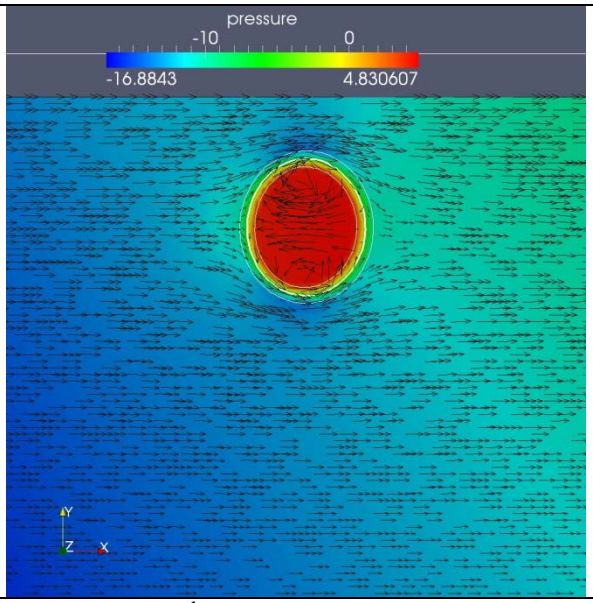

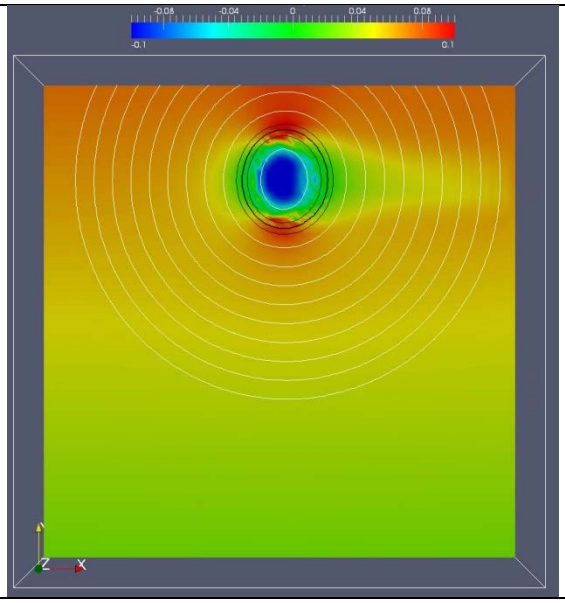

Shear rate: 2.0 s^{-1}
Relative velocity: 0.065 m/s
Density: 996.5/1.161 (kg/m^3)
Viscosity: 8.5439E-04 (liquid); 1.858E-05 (gas)
Bubble diameter: 5 mm

Force estimate is over timestep range of: 1000 - 3000
Drag control force: 0.1065 N/kg
Lift control force: 0.05175 N/kg
Drag coefficient: 0.1396
Lift coefficient: 0.2952

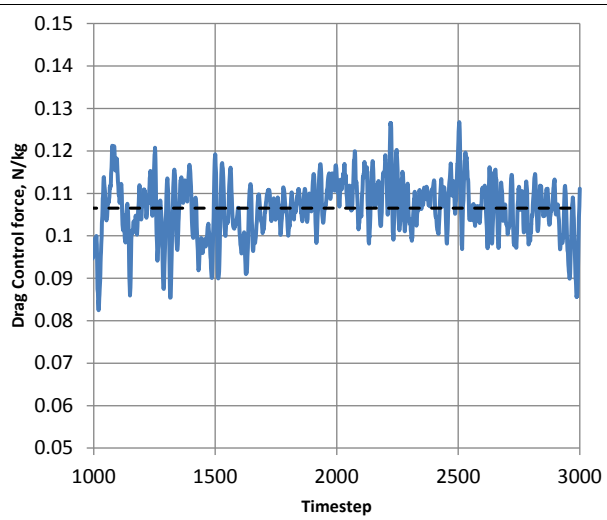

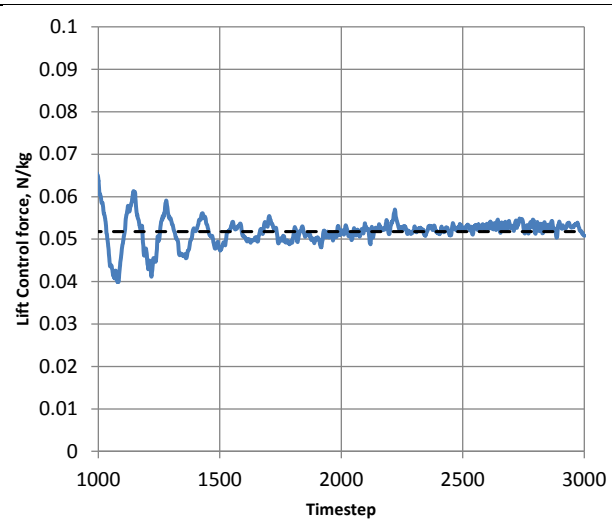

Figure 10. Summary of the SW1 case with uniform shear of 2.0. Bubble is located 1 radius from the top free-slip wall.

<u>Case NSW0.5</u>: The detailed information for this case is summarized in the following table.

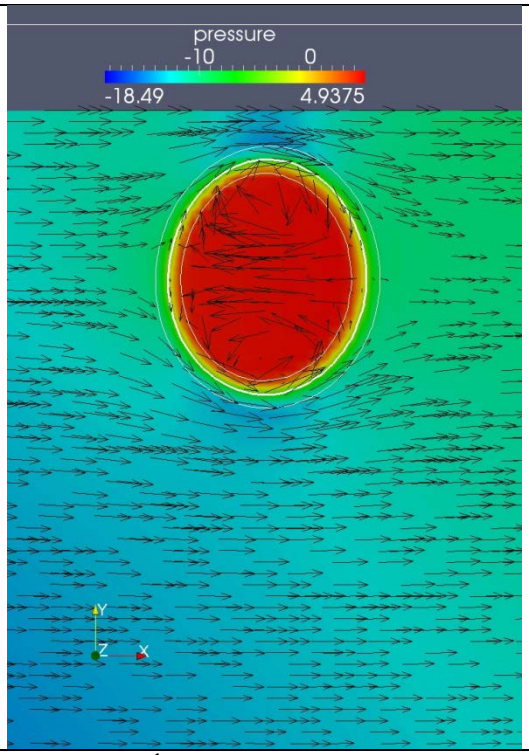

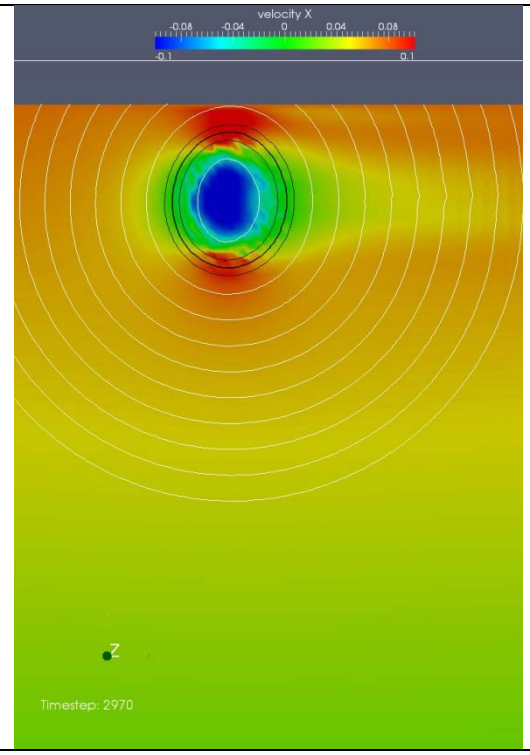

Shear rate: 2.0 s^{-1}
Relative velocity: 0.0675 m/s
Density: 996.5/1.161 (kg/m^3)
Viscosity: 8.5439E-04 (liquid); 1.858E-05 (gas)
Bubble diameter: 5 mm

Force estimate is over timestep range of: 1000 - 3000
Drag control force: 0.11850 N/kg
Lift control force: 0.08897 N/kg
Drag coefficient: 0.1440
Lift coefficient: 0.4888

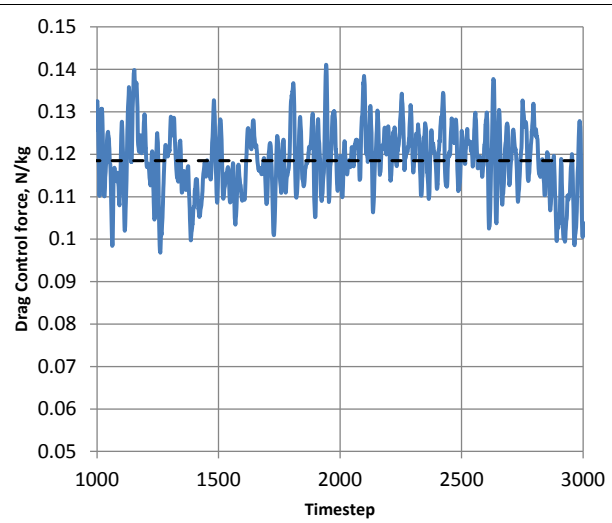

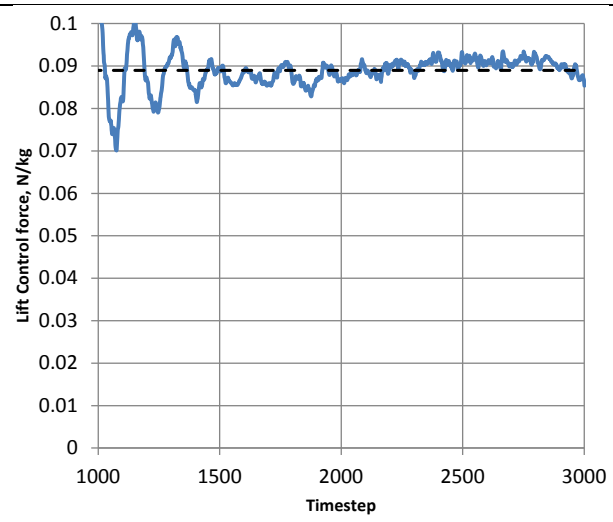

Figure 11. Summary of the NSW0.5 case with uniform shear of 2.0. Bubble is located half the radius from the top no-slip wall.

Case SW0.5: The detailed information for this case is summarized in the following table.

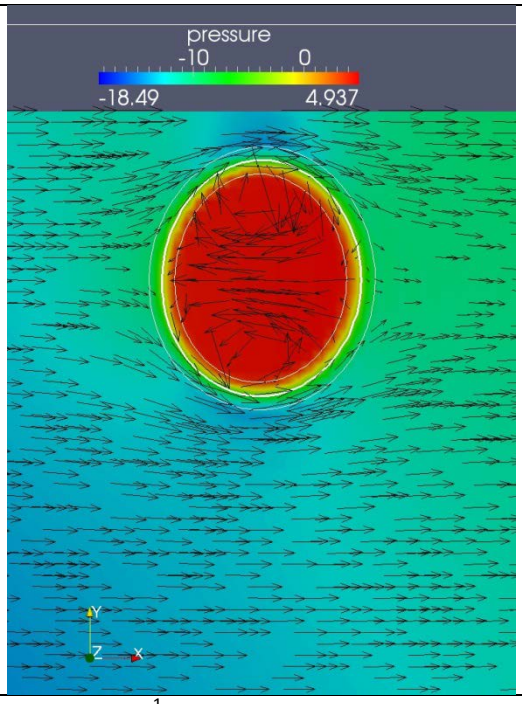

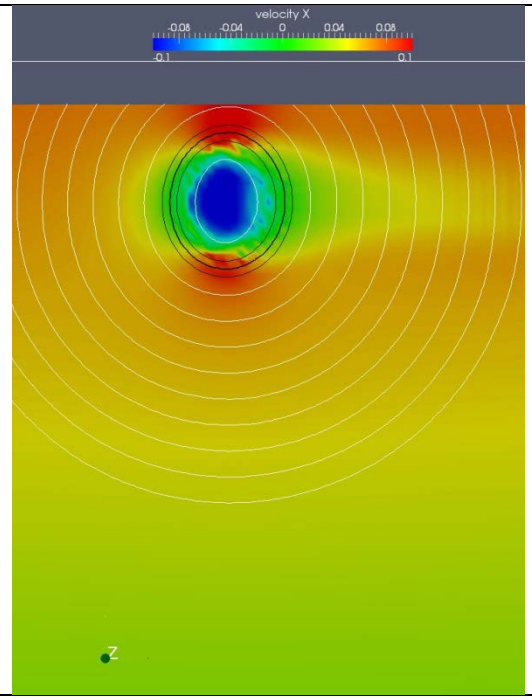

Shear rate: 2.0 s^{-1}
Relative velocity: 0.03375 m/s
Density: 996.5/1.161 (kg/m^3)
Viscosity: 8.5439E-04 (liquid); 1.858E-05 (gas)
Bubble diameter: 5 mm

Force estimate is over timestep range of: 1000 - 3000
Drag control force: 0.11308 N/kg
Lift control force: 0.08271 N/kg
Drag coefficient: 0.1374
Lift coefficient: 0.4544

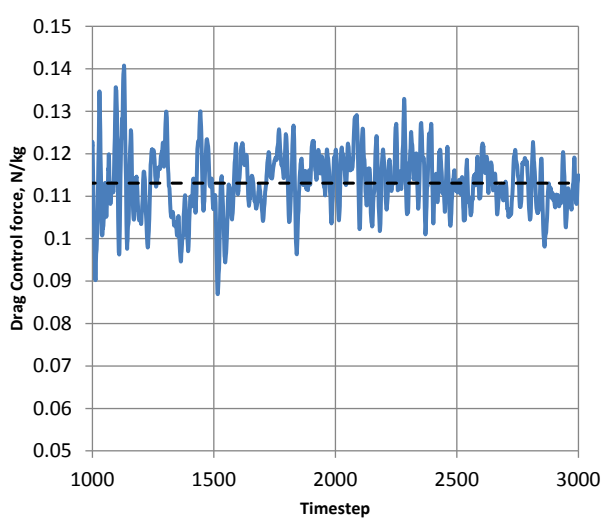

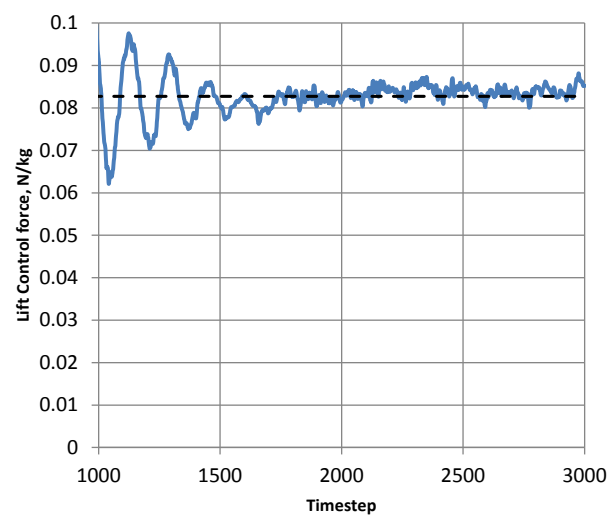

Figure 12. Summary of the SW0.5 case with uniform shear of 2.0. Bubble is located half the radius from the top free-slip wall.

<u>Case NSW0.25</u>: The detailed information for this case is summarized in the following table.

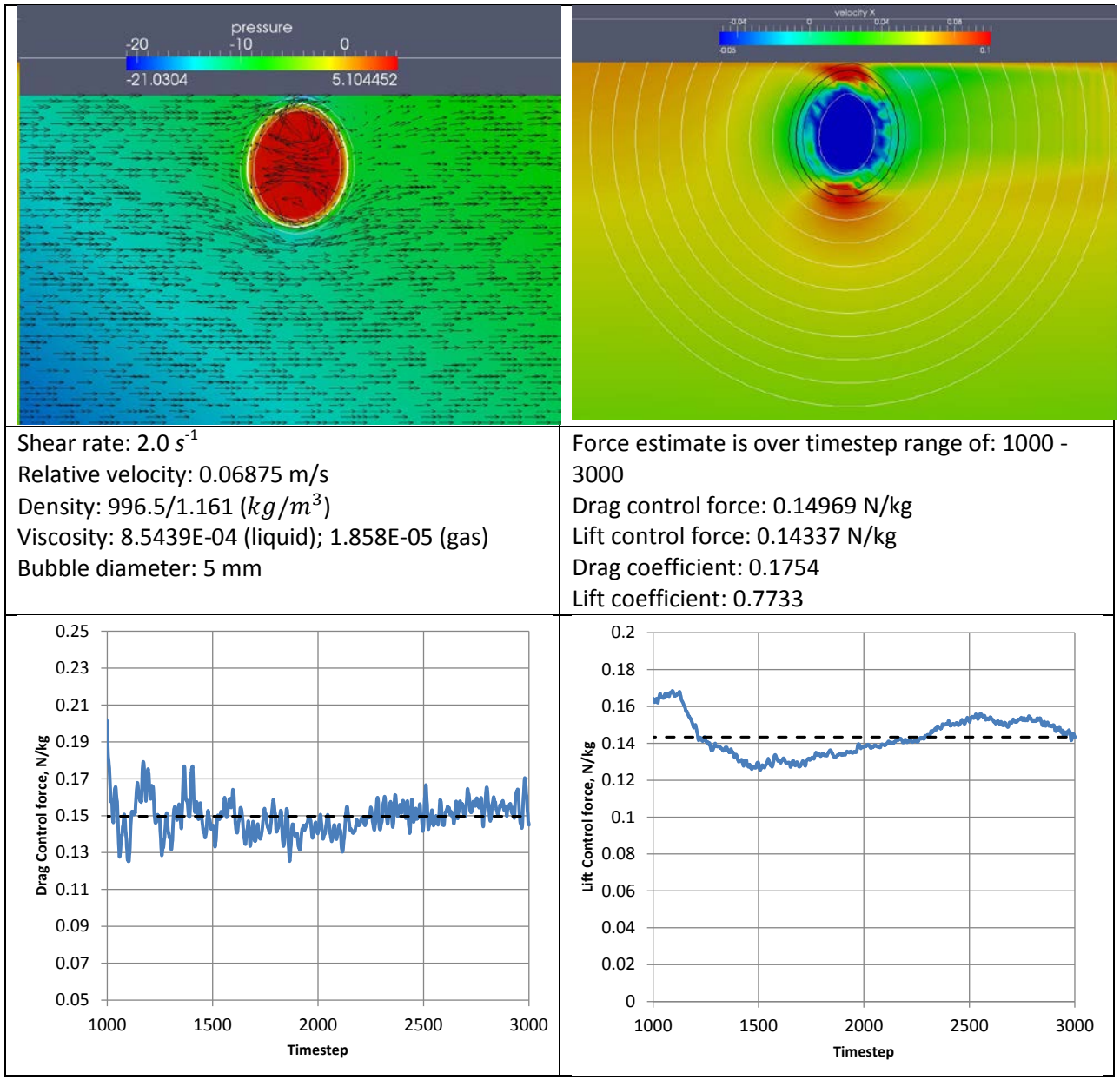

Figure 13. Summary of the NSW0.25 case with uniform shear of 2.0. Bubble is located one quarter of the radius from the top no-slip wall.

<u>Case ONSW1</u>: The detailed information for this case is summarized in the following table.

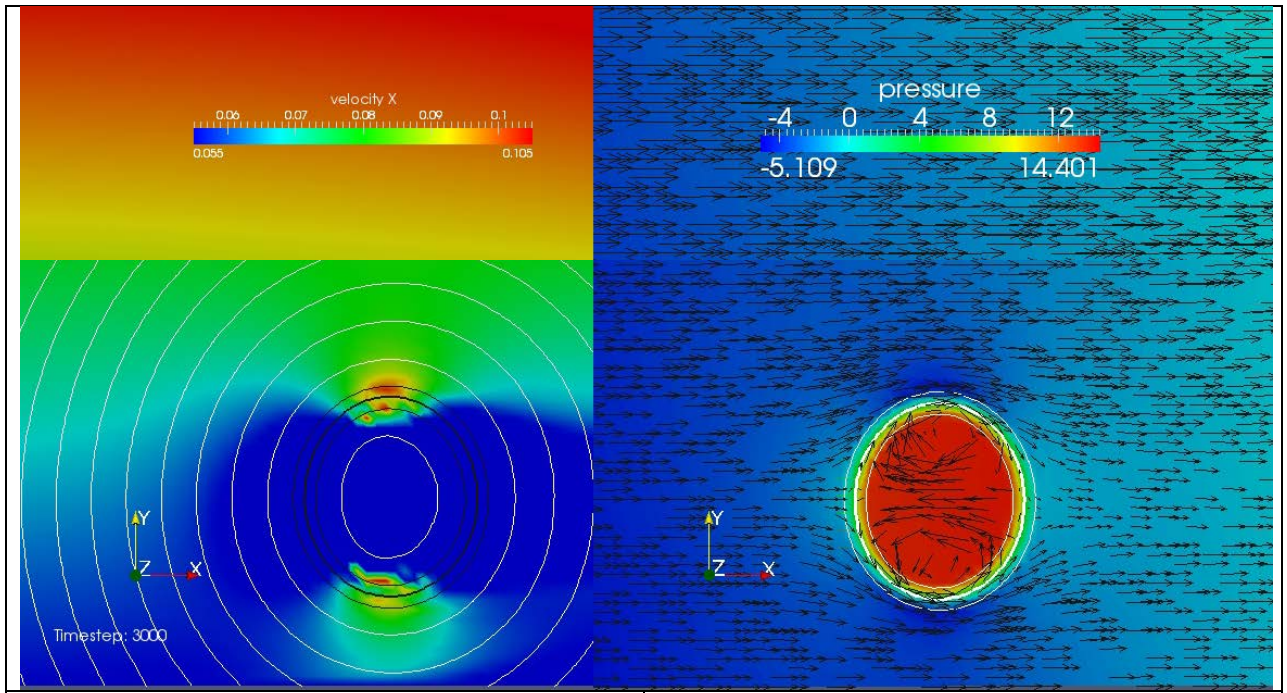

Shear rate: 2.0 s^{-1} Relative velocity: 0.065 m/s Density: 996.5/1.161 (kg/m^3) Viscosity: 8.5439E-04 (liquid); 1.858E-05 (gas) Bubble diameter: 5 mm	Force estimate is over timestep range of: 1000 - 3000 Drag control force: 0.13396 N/kg Lift control force: 0.03396 N/kg Drag coefficient: 0.1756 Lift coefficient: 0.1938

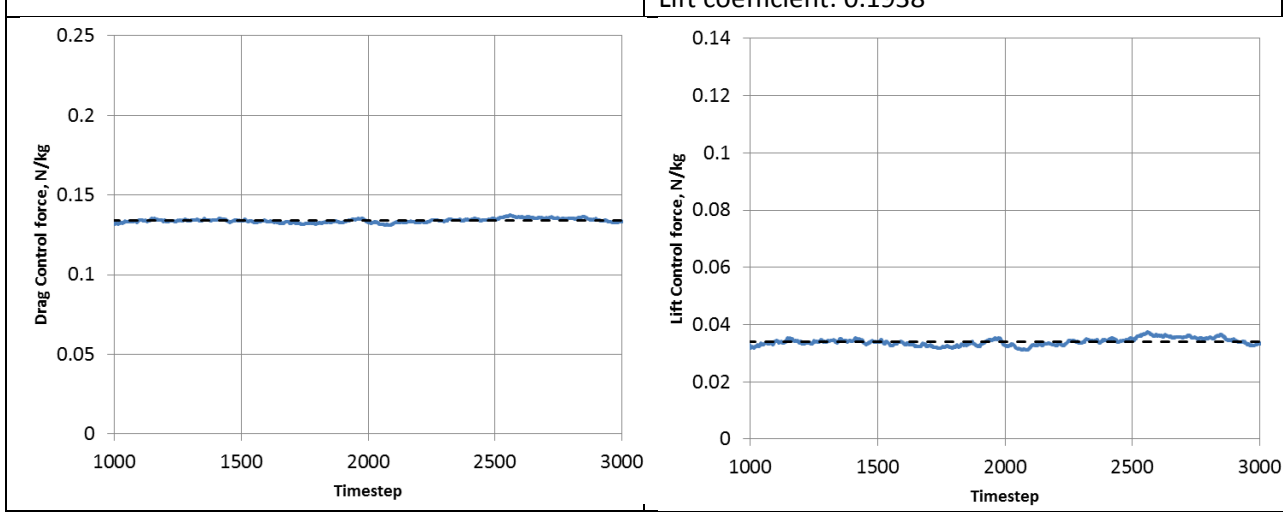

Figure 14. Summary of the ONSW1 case with uniform shear of 2.0. Bubble is located one radius from the bottom no-slip wall. Top part of the domain was cut off to show the details and legend.

<u>Case ONSW0.5</u>: The detailed information for this case is summarized in the following table.

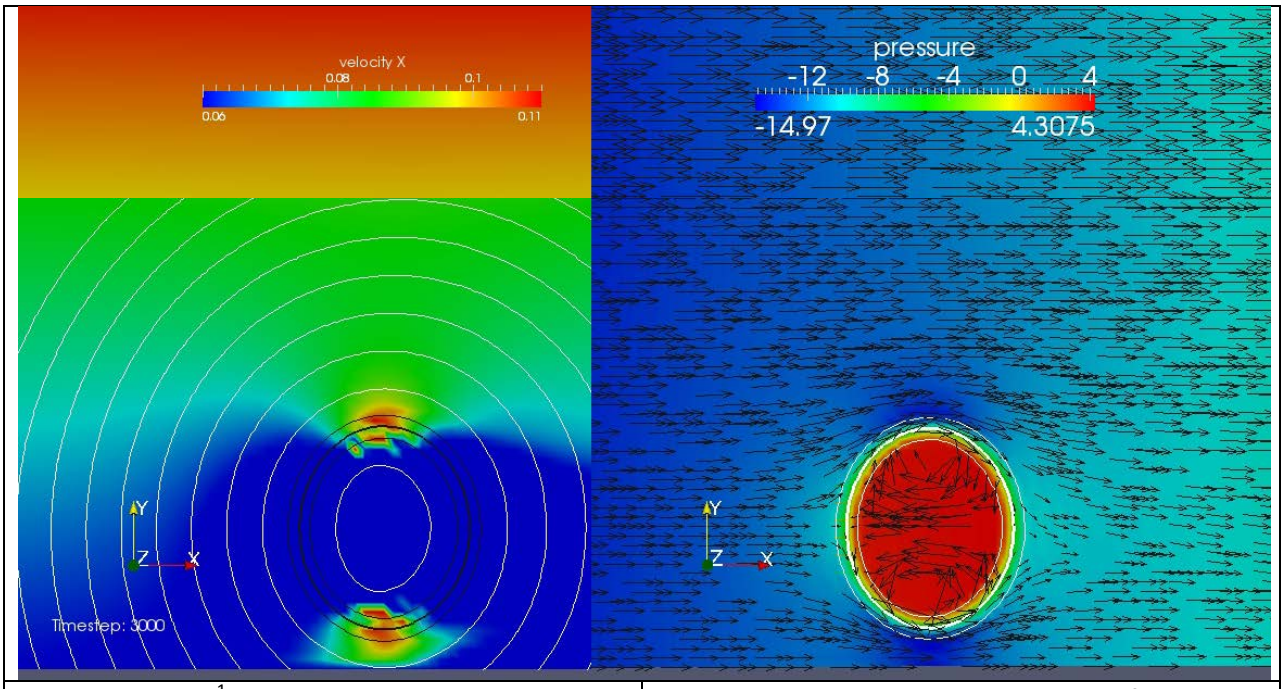

Shear rate: 2.0 s^{-1} Relative velocity: 0.0675 m/s Density: 996.5/1.161 (kg/m^3) Viscosity: 8.5439E-04 (liquid); 1.858E-05 (gas) Bubble diameter: 5 mm	Force estimate is over timestep range of: 1000 - 3000 Drag control force: 0.10350 N/kg Lift control force: 0.00350 N/kg Drag coefficient: 0.1258 Lift coefficient: 0.0192

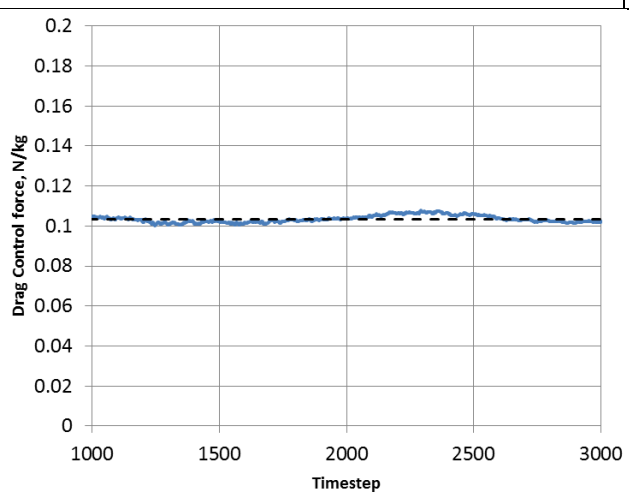

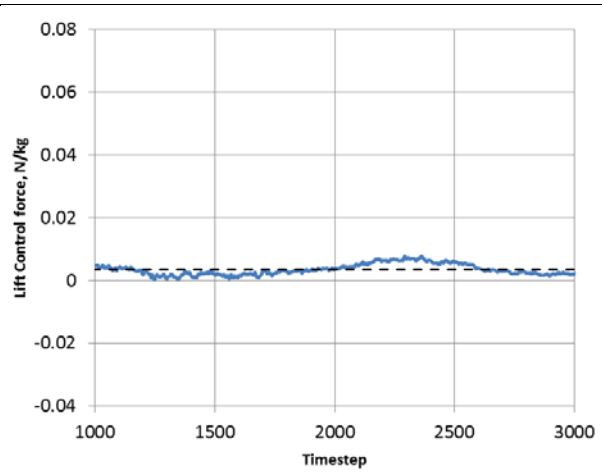

Figure 15. Summary of the ONSW0.5 case with uniform shear of 2.0. Bubble is located half the radius from the bottom no-slip wall.

<u>Case ONSW0.25</u>: The detailed information for this case is summarized in the following table.

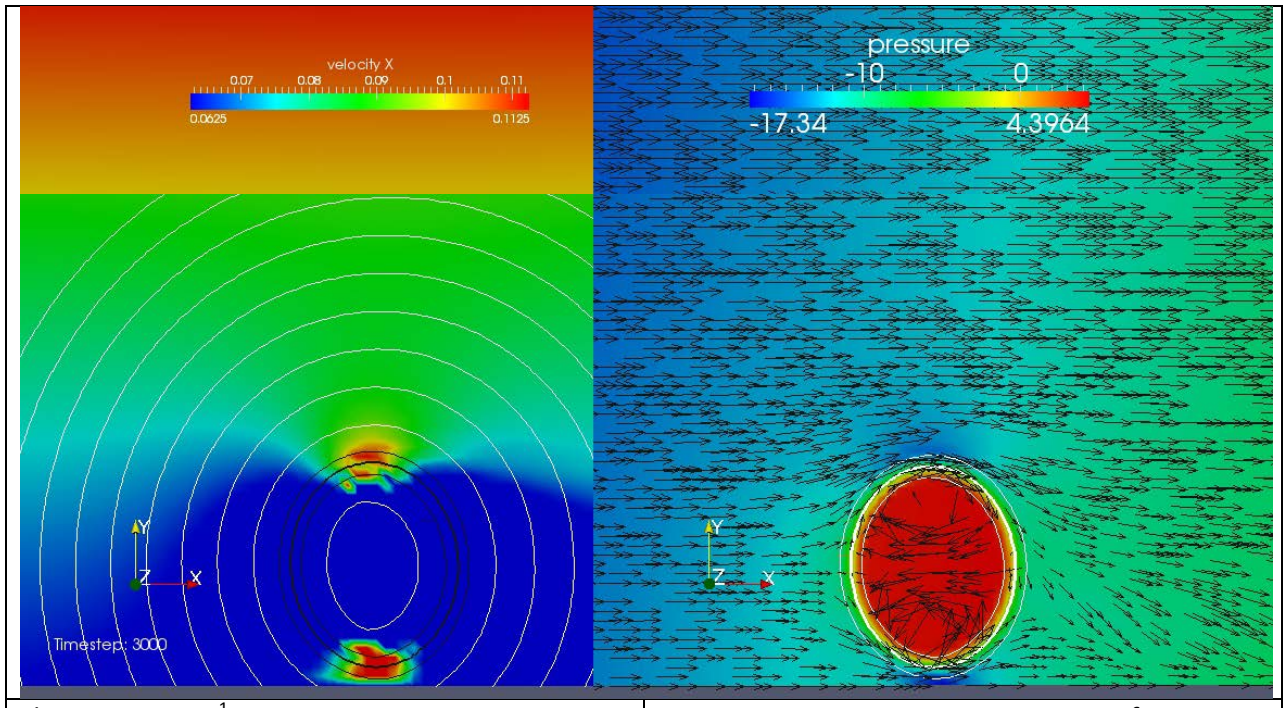

Shear rate: 2.0 s^{-1} Relative velocity: 0.06875 m/s Density: 996.5/1.161 (kg/m^3) Viscosity: 8.5439E-04 (liquid); 1.858E-05 (gas) Bubble diameter: 5 mm	Force estimate is over timestep range of: 4000 - 10000 Drag control force: 0.06853 N/kg Lift control force: -0.03147 N/kg Drag coefficient: 0.0803 Lift coefficient: -0.1697

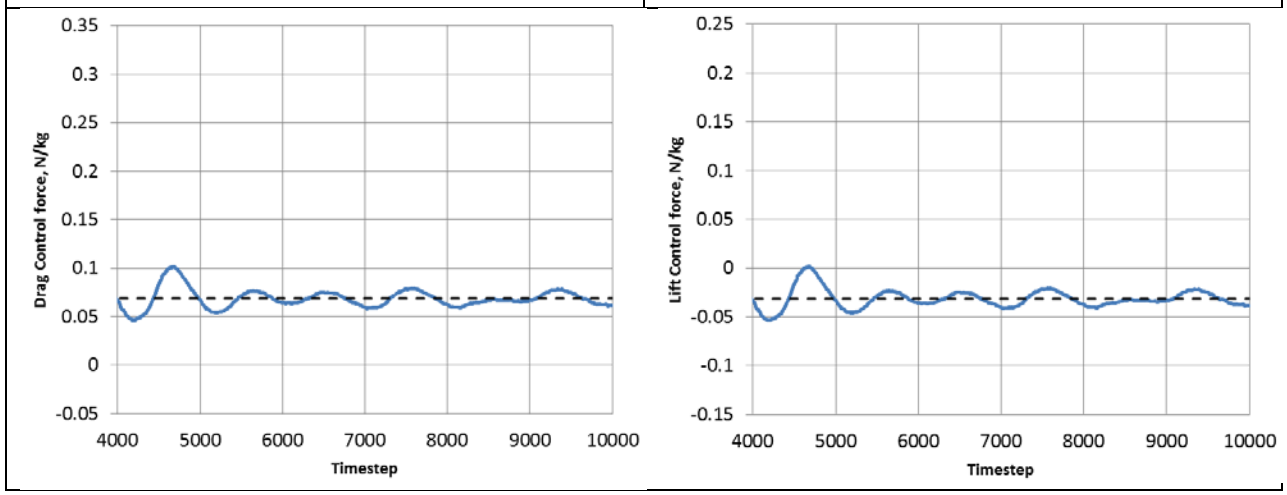

Figure 16. Summary of the ONSW0.25 case with uniform shear of 2.0. Bubble is located a quarter of the radius from the bottom no-slip wall.

By combining the results for the lift coefficient in the cases SW and NSW series, we can obtain the effect of the wall dependence, which is presented in Figure 17. Note, that the PHASTA case set-up effectively represents the downflow pattern, and thus the lift force pushes the bubble away from the "top" (faster moving) wall. This way as the bubble approaches the wall, the effect of wall proximity only increases the lift coefficient.

On the other side of the domain, the bubble experience the opposite effect (see cases "Opposite No-Slip Wall (ONSW)" – 1, 0.5 and 0.25 in Figures 14 through 16). We have summarized the observed lift coefficients as a function of the distance from the top wall in Figure 17. Note that the lift coefficient changes sign from positive to negative when the distance to the bottom wall goes from ½ bubble radius to ¼ radius. For the conditions under consideration, one can interpolate that the wall effect balances the lift force due to uniform shear at 3/8 bubble radius distance from the wall (e.g. the average lateral control force is expected to be near zero at this location). As can be seen from Figure 16, the control force demonstrates unstable behaviors, which represents bubble fluctuation near the wall. Note that there is a significant relative velocity of the bubble in our near wall simulations compared to those performed using FTC3D code (below).

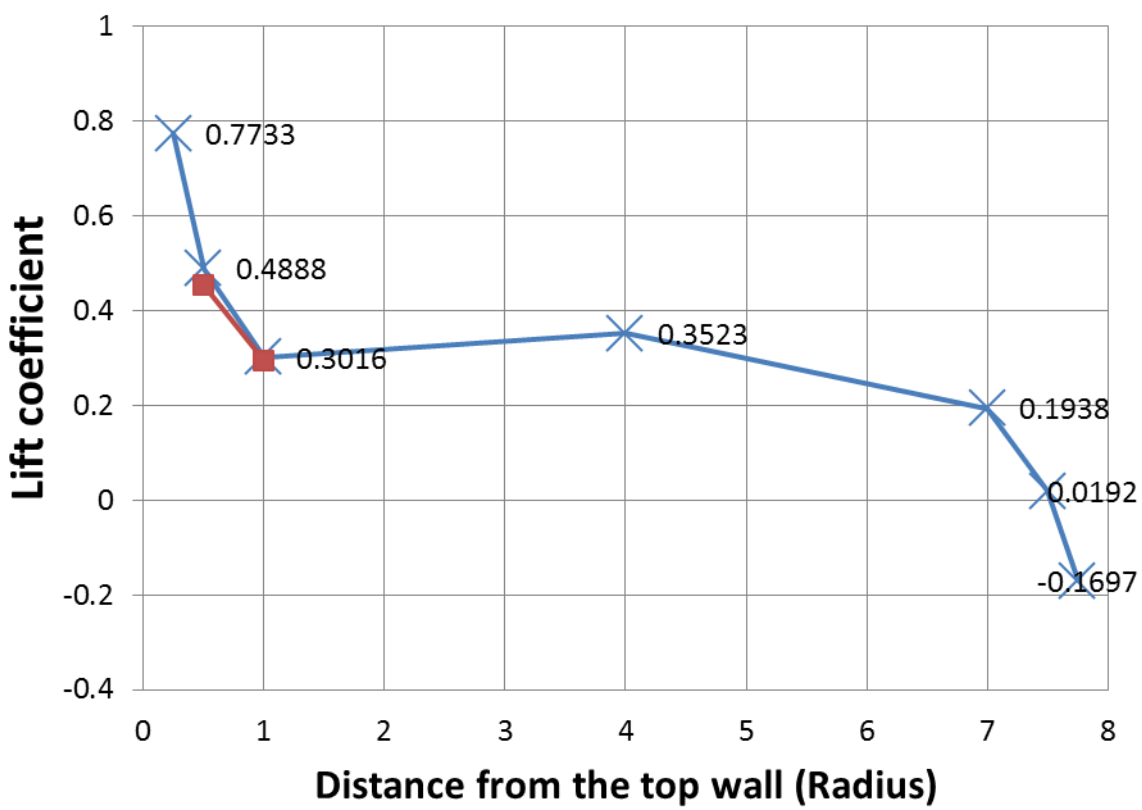

Figure 17. Lift coefficient dependence on the distance from the wall (measured in bubble radii from the closest point of the interface to the wall). Red line shows the slip-wall condition option.

6. Results for FTC3D simulations and measurements

Most of the computations done using the FTC3D code used a computational domain of size 0.5 x 0.5 x 0.25 resolved by a uniform grid of 80 x 80 x 40 points. Tests with larger domains and on finer grids, showed relatively minor changes as the domain size was increased. As discussed above, the inflow and the physical properties of the gas and the liquid were specified and the gravity acceleration in both the vertical and the horizontal direction adjusted using a PID controller to keep the bubble steady. The simulations have been run using "computational units," usually selected to be relatively close to unity. The results are then presented in dimensionless form, allowing for comparisons with physical variables. While several cases were examined, here we focus on those listed in Table 2. The deformability of the bubble was changed by changing the surface tension, the shear rate was changed by modifying the inlet and the vertical wall velocities. When the location of the bubble was changed, the inlet velocity was modified so that the slip velocity remained constant.

Figure 18 shows a nearly spherical bubble in a vertical shear flow after the flow has reached a steady state. The frame on the left shows a bubble in the middle of the channel and the frame on the right shows a bubble close to the right wall. The bubble and velocity field in a plane cutting through the bubble is shown by a quiver plot and the magnitude of the vertical velocity is shown by a color plot. In this case the surface tension is sufficiently high so the bubble remains nearly spherical. The outflow velocity is shown by arrows extending out of the domain at the bottom, where the wake of the bubble is clearly visible. The shear for the case with a bubble near the wall is smaller than for the case where the bubble is in the middle.

The gravity acceleration versus time, adjusted using a PID controller in such a way that the bubble remains stationary, is shown in Figure 19. The top frame shows the horizontal acceleration, which is balanced by the lift on the bubble, and the bottom frame shows the vertical acceleration which in balanced by the drag. By adjusting the gravity acceleration so that the bubble remains stationary, the slip velocity is determined by the velocity at the inlet, at the horizontal location of the bubble centroid. Both the vertical and horizontal acceleration initially overshoots its final value, but by adjusting the control parameters both components generally converge rapidly.

It is by now well known that the bubble deformability determines the lift force that acts on a bubble rising in vertical shear. A nearly spherical bubble rising near a wall in upflow is pushed toward the wall while a more deformable bubble is pushed away from it. This can have profound implications for the overall structure of the flow, affecting both the overall pressure drop and flow rate as well as the mixing that takes place. In Figure 20 we plot the lift and drag coefficients versus the Eotvos (Eo) number. While the drag coefficient increases rapidly with the deformability (increasing Eo), the lift coefficient decreases. The lift coefficient is positive for low Eo (lift toward the wall) and becomes negative as Eo increases. As Eo goes to zero, the lift coefficient levels off slightly and we would expect it, as well as the drag, to eventually become independent of the Eo. For the case examined the value for the lowest Eo is 0.365, which is slightly higher than the value reported by Tomiyama et al. (2002), but not by much. In general we find that as the bubbles become nearly spherical the lift coefficient is slightly above 0.3.

One of the key questions for bubbles in a shear flow is the dependency of the lift and drag coefficient on the shear rate. In Figure 21 the lift (a) and drag (b) coefficients are plotted versus shear rate. For the shear rates examined here, the dependency is obviously weak. However, both fall off slightly as the shear rate increases, suggesting that it is important to examine higher values as well. For given physical parameters, stronger shear is likely to deform the bubbles more and that will reduce the lift and possibly the drag.

In Figure 22 we examine the effect of the distance to the wall on the lift (a) and drag (b) force on the bubbles. We show results for three sets of runs, where only difference is the value of the surface tension. The red curve is for the most deformable bubble and the black curve is for the least deformable one. When the bubbles are far from the wall they all experience a lift force pushing them to the wall, but as they come within about a diameter from the wall, the lift changes sign and pushes them away. As expected, the most deformable bubbles has the highest drag and lowest lift, when it is in the middle of the channel, but as it is moved closer to the wall the force pushing the deformable bubble is pushed away from the wall is higher. Notice that the deformable bubble “feels” the wall earlier than the more rigid ones. The drag force on the bubbles increases as they are moved to the wall but the deformable bubble continues to experience the largest drag.

The Reynolds number for the cases shown here have been relatively modest. We have also examined higher Reynolds numbers, both by changing the viscosity or the inflow velocity. As the Reynolds number increases the time to reach a steady state increases, but our results so far indicate that they will eventually settle down. It is also possible that the transient can be shortened by a different selection of the control parameters. Figure 23 shows the lift (a) and drag (b) force on the bubbles versus distance to the wall. While the results are similar to the lower Reynolds number case in Figure 22, here we see that the lift and the drag forces remains essentially constant until the bubble is very close to the wall. The drag coefficient is also lower, as expected.

Table 2. The various parameters used for the FTC3D baseline case.

Viscosity (Fluid/Bubble)	0.01 / 0.001
Wall Velocity	Vwest = -2.0 Veast = -3.0
Shear Reynolds Number G_R	2.0
Relative velocity of bubble	2.5
Bubble's Reynolds Number Re_b	**25.0**
Capillary Number Ca	0.004
Mean x-force	-1.45
Mean y-force	86.72
Froud Number Squared Fr^2	0.00461
Eotvos Number Eo	1.69
Morton Number M	6.76e-6
LogM	-5.17
Lift coefficient	**0.283**
Drag Coefficient	**1.803**

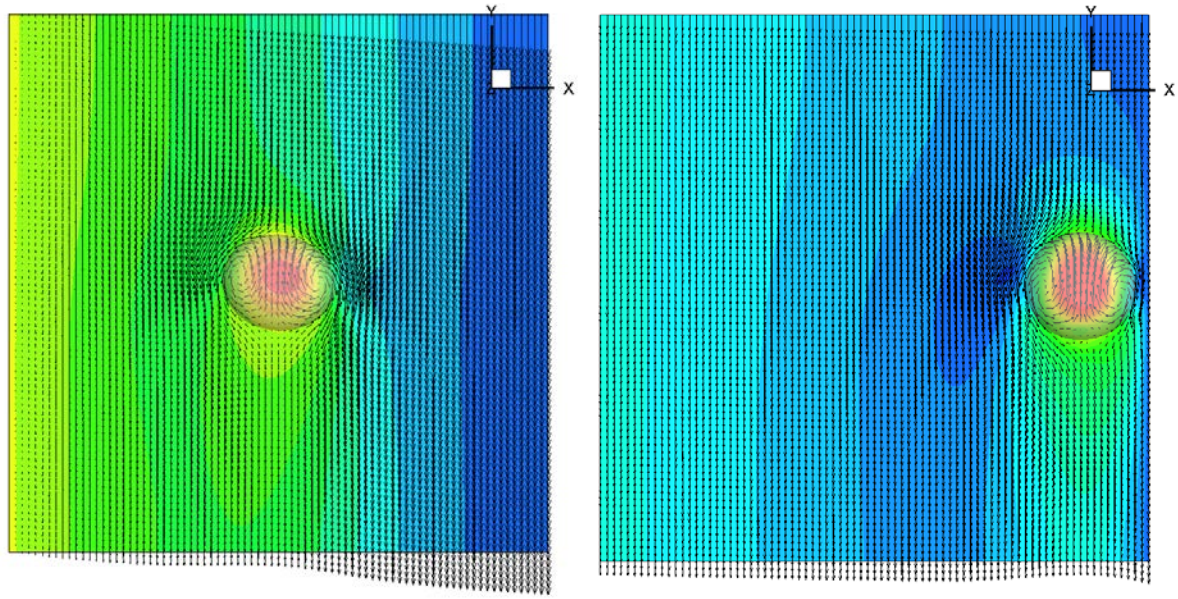

Figure 18. The bubble and the velocity field shown by a quiver plot. The color indicates the vertical velocity component. In the left frame the bubble is in the middle of the domain and in the right frame the bubble is close to the right wall.

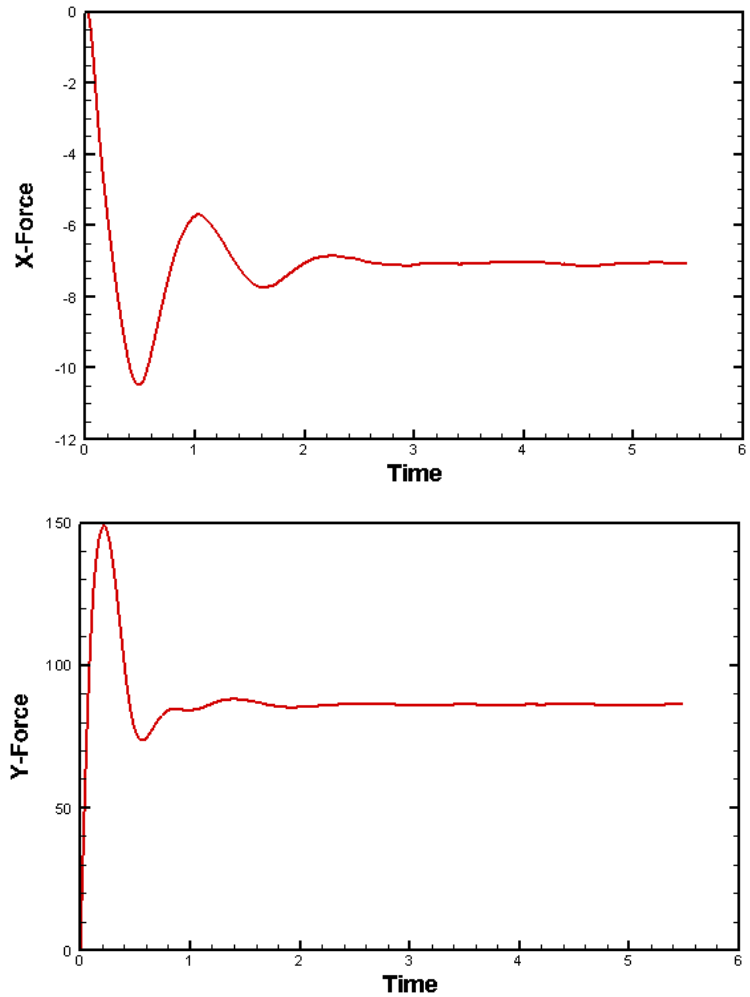

Figure 19. The horizontal (top) and the vertical (bottom) component of the gravitational acceleration versus time, as adjusted by the PID controllers to keep the bubble stationary.

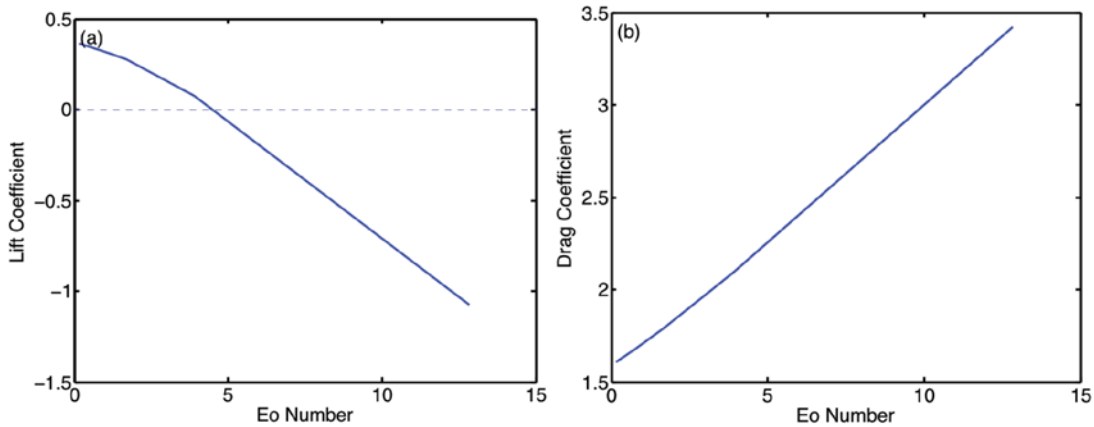

Figure 20. The lift and drag coefficients versus the Eotvos (Eo) number.

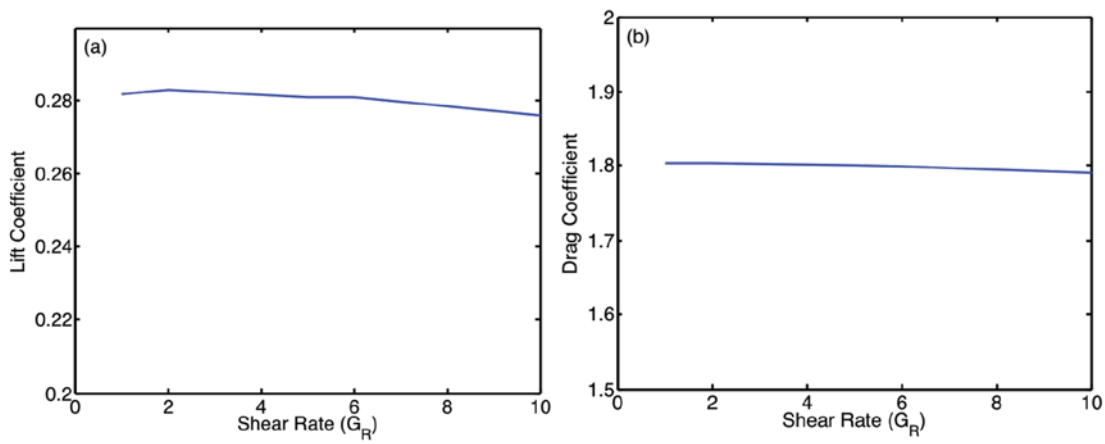

Figure 21. The lift (a) and drag (b) coefficient versus shear rate.

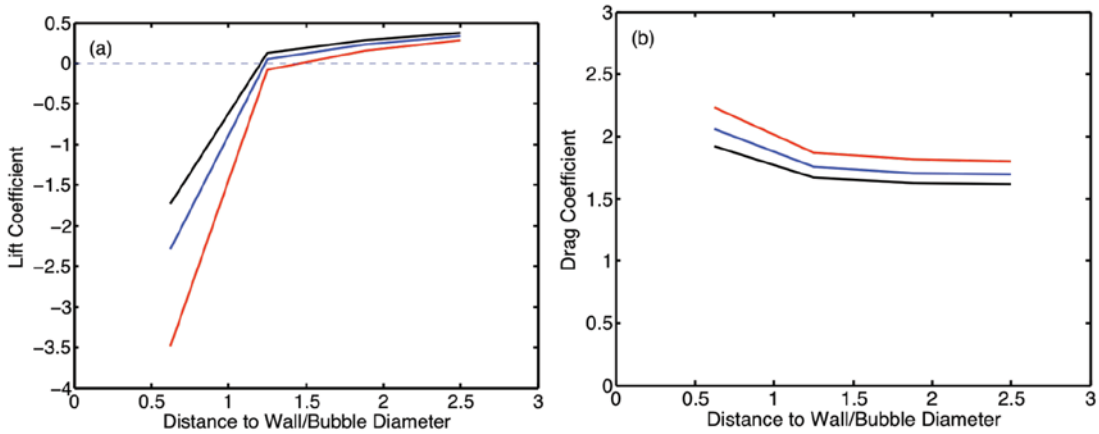

Figure 22. The effect of the distance to the wall on the lift (a) and drag (b) force on the bubbles.

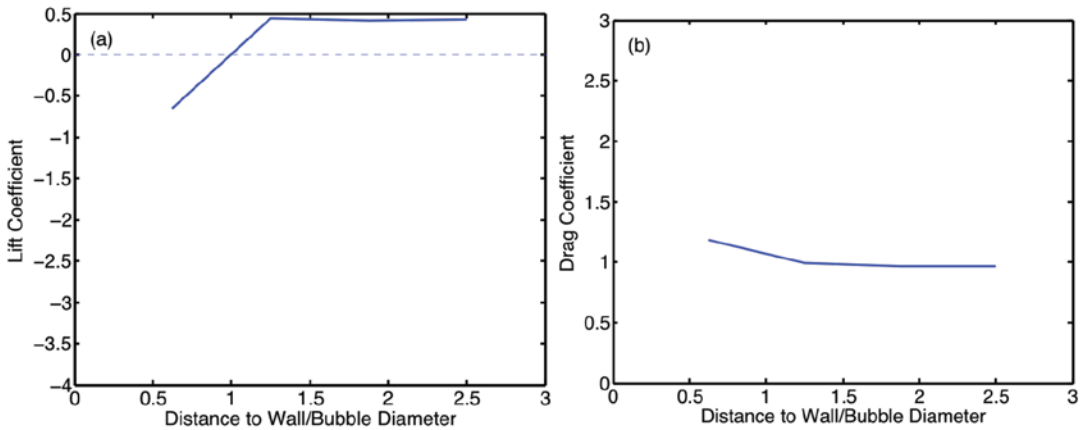

Figure 23. The effect of the distance to the wall on the lift (a) and drag (b) force on the bubbles for a bubble Reynolds number = 50.

7. Future Work

The results shown here suggest that the strategy used here to obtain the lift and drag on individual bubbles is reasonably effective. However, two issues have emerged that we expect to address in a follow-on study:

- The current setup, where the inflow is specified and we apply outflow boundary conditions at the bottom boundary, limits the amount of shear that we can examine, since the outflow boundary conditions are not designed for backflow thorough the outflow boundary. We believe that we can overcome this limitation by specifying the flow profile at the outflow boundary and using a longer computational domain to limit the effect of the boundary on the wake. This was demonstrated for some of the presented case using PHASTA code: SW5, SW10 and SW50 (including negative inflow velocity profile to maintain low relative velocity at high shear rate).
- The current approach to keep the vertical position of the bubble in the middle of the computational domain by adjusting the vertical gravitational acceleration results in a change in the various nondimensional numbers that control the flow when the horizontal location is changed. The Reynolds number is constant, but the more physical situation is if the Reynolds number varies but the Eotvos and the Morton number stay the same. We should be able to do so by using a sliding domain that moves with the bubble. That would allow us to fix the value of the vertical gravitational component and adjust only the horizontal one.

Given that significant effort was put into the development of additional tools used for the presented studies, it makes good sense to continue the work by expanding the parametric space. The authors will value the feedback from the modeling community with regards to specific gaps which exist in the available experimental database where the DNS/ITM approach can help.

Bibliography

Bolotnov, I. et al., 2011. Detached Direct Numerical Simulation of Turbulent Two-phase Bubbly Channel Flow. *Int. J. Multiphase Flow,* Volume 37, pp. 647-659.

Biswas, S., Esmaeeli, A. & Tryggvason, G. 2005 Comparison of results from DNS of bubbly flows with a two-fluid model for two-dimensional laminar flows. Int. J. Multiphase Flows 31, 1036–1048.

Brackbill, J. U., Kothe, D. B. & Zemach, C., 1992. A continuum method for modeling surface tension. *J. Computational Physics,* 100(2), pp. 335-354.

Bunner, B. & Tryggvason, G. 2002a Dynamics of homogeneous bubbly flows. Part 1. Rise velocity and microstructure of the bubbles. J. Fluid Mech. 466, 17–52.

Bunner, B. & Tryggvason, G. 2002b Dynamics of homogeneous bubbly flows. Part 2. Velocity fluctuations. J. Fluid Mech. 466, 53–84.

Bunner, B. & Tryggvason, G. 2003 Effect of bubble deformation on the stability and prop- erties of bubbly flows. J. Fluid Mech. 495, 77–118.

Esmaeeli, A. & Tryggvason, G. 2005 A direct numerical simulation study of the buoyant rise of bubbles at O(100) Reynolds number. Phys. Fluids 17, 093303.

Dijkhuizen, W., Roghair, I., Annaland, M. Van Sint & Kuipers, J. 2010a DNS of gas bubbles behaviour using an improved 3d front tracking model–drag force on isolated bubbles and comparison with experiments. Chem. Eng. Sci. 65, 1415–1426.

Dijkhuizen, W., Roghair, I., Annaland, M. Van Sint & Kuipers, J. 2010b DNS of gas bubbles behaviour using an improved 3d front tracking model–model development. Chem. Eng. Sci. 65, 1427–1437.

Hao, Y. & Prosperetti, A. 2004 A numerical method for three-dimensional gas–liquid flow computations. J. Comput. Phys. 196, 126–144.

Hua, J. & Lou, J. 2007 Numerical simulation of bubble rising in viscous liquid. J. Comput. Phys. 222, 769–795.

Jansen, K. E., 1993. Unstructured grid large eddy simulations of wall bounded flows. *Annual Research Briefs, Center for Turbulence Research, NASA Ames/Stanford University,* p. 151.

Jansen, K. E., 1999. A stabilized finite element method for computing turbulence. *Comp. Meth. Appl. Mech. Eng.,* Volume 174, pp. 299-317.

Muradoglu, M. & Kayaalp, A. D. 2006 An auxiliary grid method for computations of multiphase flows in complex geometries. J. Comput. Phys. 214, 858–877.

Nagrath, S., Jansen, K. E., Lahey, R. T. & Akhatov, I., 2006. Hydrodynamic simulation of air bubble implosion using a FEM based level set approach. *Journal of Computational Physics,* Volume 215, pp. 98-132.

Sahni, O. et al., 2006. Efficient anisotropic adaptive discretization of the cardiovascular system. *Computer Methods in Applied Mechanics and Engineering,* 195(41-43), pp. 5634-5655.

Sethian, J. A., 1999. *Level set methods and fast marching methods.* s.l.:Cambridge University Press.

Sussman, M. et al., 1999. An adaptive level set approach for incompressible two-phase flows. *J. Computational Physics,* 148(1), pp. 81-124.

Sussman, M. & Fatemi, E., 1999. An efficient, interface-preserving level set re-distancing algorithm and its application to interfacial incompressible fluid flow. *Siam J. on Scientific Computing,* 20(4), pp. 1165-1191.

Sussman, M., Fatemi, E., Smereka, P. & Osher, S., 1998. An improved level set method for incompressible two-phase flows. *J. Computers & Fluids,* 27(5-6), pp. 663-680.

Sussman, M. & Smereka, P., 1997. Axisymmetric free boundary problems. *J. Fluid Mech.,* Volume 341, pp. 269-294.

Tejada-Martinez, A. E. & Jansen, K. E., 2005. A parametric-free dynamic subgrid-scale model for large-eddy simulation. *Computer Methods in Applied Mechanics and Engineering,* 194(9), pp. 1225-1248.

Tomiyama, A., Tamai, H., Zun, I. & Hosokawa, S. 2002 Transverse migration of single bubbles in simple shear flows. Chem. Eng. Sci. 57, 1849–1858.

Tryggvason, G., Bunner, B., Esmaeeli, A., Juric, D., Al-Rawahi, N., Tauber, W., Han, J., Nas, S. & Jan, Y.-J. 2001 A front tracking method for the computations of multiphase flow. J. Comput. Phys. 169, 708–759.

Tryggvason, G., Scardovelli, R. & Zaleski 2011 Direct Numerical Simulations of Gas- Liquid Multiphase Flow. Cambridge University Press.

Unverdi, S. O. & Tryggvason, G. 1992 A front-tracking method for viscous, incompressible, multi-fluid flows. J. Comput. Phys. 100, 25–37.

van Sint Annaland, M., Dijkhuizen, W., Deen, N.G. & Kuipers, J.A.M. 2006 Numerical simulation of gas bubbles behaviour using a 3D front tracking method. AIChE J. 52, 99–110.

Whiting, C. H. & Jansen, K. E., 2001. A stabilized finite element formulation for the incompressible Navier-Stokes equations using a hierarchical basis. *International Journal of Numerical Methods in Fluids,* Volume 35, pp. 93-116.

Zhou, M. et al., 2010. Cardiovascular flow simulation at extreme scale. *Comput. Mech.,* Volume 46, pp. 71-82.